

1 A new balance formula to estimate new particle formation rate: reevaluating the effect of coagulation scavenging

2 Runlong Cai and Jingkun Jiang*

3 State Key Joint Laboratory of Environment Simulation and Pollution Control, School of Environment, Tsinghua University,
4 Beijing, 100084, China

5 * Correspondence to: J. Jiang (jiangjk@tsinghua.edu.cn)

6 **Abstract.** A new balance formula to estimate new particle formation rate is proposed. It is derived from aerosol general
7 dynamic equation in the discrete form and then converted into an approximately continuous form for analysing data from new
8 particle formation (NPF) field campaigns. The new formula corrects the underestimation of the coagulation scavenging effect
9 occurred in the previously used formulae. It also clarifies the criteria in determining the upper size bound in measured aerosol
10 size distributions for the estimating new particle formation rate. A NPF field campaign was carried out from March 7th to Apr.
11 7th, 2016, in urban Beijing, and a diethylene glycol scanning mobility particle spectrometer equipped with a miniature
12 cylindrical differential mobility analyser was used to measure aerosol size distributions down to ~1 nm. 11 typical NPF events
13 were observed during this period. Measured aerosol size distributions from 1 nm to 10 μm were used to test the new formula
14 and formulae used widely in the literature. The previously used formulae that perform well in relatively clean atmosphere
15 where nucleation intensity is not strong were found to underestimate the comparatively high new particle formation rate in
16 urban Beijing because of their underestimation or neglect of the coagulation scavenging effect. The coagulation sink term is
17 the governing component of the estimated formation rate in the observed NPF events in Beijing, and coagulation among newly
18 formed particles contributes a large fraction to the coagulation sink term. Previously reported formation rates in Beijing and
19 in other locations with intense NPF events might be underestimated because the coagulation scavenging effect was not fully
20 considered, e.g., estimated formation rates of 1.5 nm particles in this campaign using the new formula are 1.3 – 4.3 times those
21 estimated using the formula neglecting coagulation among particles in the nucleation mode.

22 1 Introduction

23 New particle formation (NPF) is a frequently occurring phenomenon in atmospheric environment. In a typical NPF event,
24 gaseous precursors burst out into particles due to nucleation and lead to a rapid increase in atmospheric aerosol population.
25 Nucleated particles can grow quickly to increase the number concentration of cloud condensation nuclei (Kerminen et al.,
26 2012; Kuang et al., 2009; Leng et al., 2014) and thus has indirect impacts on radiative forcing and global climate (Lohmann
27 & Feichter, 2005). Continuous growth of nucleated particles also provides increasing aerosol surface area for heterogeneous
28 physicochemical processes. NPF studies can trace back to the early 20th century (Aitken, 1911) and NPF events have been
29 observed in various atmospheric environment, e.g., from city to countryside, from desert (Misaki, 1964) to rain forest (Zhou,

30 2002), from continent to the ocean (Covert et al., 1992), from the equator (Clarke et al., 1998) to polar area (Covert et al.,
31 1996; Park et al., 2004), and from troposphere to stratosphere (Lee et al., 2003).

32 The formation rate at which the growth flux past a certain diameter is a key parameter to quantitatively describe NPF events.
33 Different formulae have been used to estimate new particle formation rate from measured aerosol size distributions and they
34 mainly originate from two approaches. One is from the definition of nucleation rate (Heisler & Friedlander, 1977; Weber et
35 al., 1996) and the other is a population balance method (Kulmala et al., 2001; Kulmala et al., 2012). Consistency of these two
36 approaches was tested using a numerically simulated NPF event and a relative error of less than 20% was reported (Vuollekoski
37 et al., 2012). The simulated NPF event had a maximum formation rate of less than $1 \text{ cm}^{-3} \text{ s}^{-1}$. However, the reported formation
38 rates in the atmosphere vary in a large scale, e.g., approximately from 10^{-2} to $10^4 \text{ cm}^{-3} \text{ s}^{-1}$ (Kulmala et al., 2004). Suffering
39 from the assumptions made in these two approaches, their validity in describing NPF events with high formation rate needs to
40 be further explored. A high fraction of newly formed particles is scavenged by coagulation before they grow into larger sizes.
41 Both approaches potentially underestimate the contribution of the coagulation scavenging effect when calculating the
42 formation rate from measurement data. They may perform well in clean atmospheric environment where nucleation intensity
43 is not strong and aerosol concentration is relatively low, i.e., the coagulation scavenging effect is less important.

44 The effect of coagulation scavenging is more prominent when estimating the formation rate of sub-3 nm particles because of
45 their high diffusivities and high concentrations during NPF events. Due to instrument limitations, aerosol size distributions of
46 sub-3 nm particles were not available in many previous NPF field campaigns. Recent developments in diethylene glycol (DEG)
47 condensation particle counters (CPC, Iida et al., 2009; Vanhanen et al., 2011) made it feasible to develop new scanning
48 mobility particle spectrometers (SMPS) for extending aerosol size distribution measurement from ~ 3 nm down to ~ 1 nm (Jiang,
49 et al., 2011a; Franchin *et al.*, 2016). These new spectrometers were deployed in atmospheric observations (Jiang, et al., 2011b)
50 and in chamber measurements (Franchin *et al.*, 2016) to study NPF. A miniature cylindrical differential mobility analyser
51 (mini- cyDMA, Cai et al., 2017) was developed to improve the performance of the DEG-SMPS.

52 In many locations of China, high emissions lead to both high concentrations of gaseous precursors and high atmospheric
53 aerosol concentrations. NPF was frequently observed even in megacities, such as Beijing and Shanghai (Wu et al., 2007;
54 Kulmala et al., 2016; Wang et al., 2017). In most previous studies, the above population balance method was used to estimate
55 new particle formation rates in China. The reported formation rates of 3 nm particles and larger ones were typically in the
56 range of $1\text{-}10 \text{ cm}^{-3} \text{ s}^{-1}$ (Wang et al., 2013; Leng, et al., 2014; An et al., 2015; Qi et al., 2015). One study in Shanghai reported
57 a rate of 112.4 to $271.0 \text{ cm}^{-3} \text{ s}^{-1}$ for the formation of 1.5 nm particles inferred from a DEG-CPC (Xiao et al., 2015). For these
58 intense NPF events, the above balance approach may underestimate the coagulation scavenging effect and thus lead to
59 underestimation in the reported formation rate. In addition, applying new SMPSs to measure aerosol size distributions down
60 to ~ 1 nm will help to better quantify the formation rate and its governing factors in typical locations of China.

61 When estimating new particle formation rates, various particle size ranges were used in the previous formulae. The definition
62 approach tries to limit the size range towards the minimum detected diameter (Kuang *et al.*, 2008; Weber, et al., 1996), while
63 studies with the population balance method have used various size ranges. Some studies used the aerosol size distributions
64 from the minimum detected diameter up to 25 nm (Kulmala et al., 2001; Dal Maso et al., 2005; Wu et al., 2007; Wang et al.,
65 2013). Kulmala et al. (2004) recommended the upper size bound as the maximum size that the critical cluster can reach during
66 a short time interval of growth. There are also studies using narrower size ranges, such as from 3 nm to 6 nm (Sihto et al.,
67 2006; Paasonen et al., 2009; Wang et al., 2011; Vuollekoski et al., 2012) and from 1.34 nm to 3 nm (Xiao et al., 2015). In
68 principle, the estimated formation rates may vary when different particle size ranges are used. Assumptions made while
69 deriving these formulae should be fully considered when proposing criteria to choose particle size range.

70 In this study, a new population balance formula for estimating the new particle formation rate was derived from aerosol general
71 dynamic equation to properly account for the effect of coagulation scavenging, especially for analysing intense NPF events.
72 A NPF field campaign was carried out in Beijing. Aerosol size distributions down to ~ 1 nm were measured using the DEG-
73 SMPS equipped with the mini- cyDMA. Data from this campaign and from literature are used to test the new formula and
74 other widely used formulae. Different formulae are compared and their applicability in analysing intense NPF events are
75 addressed. Criteria to choose particle size range for formation rate estimation are proposed and evaluated. Governing
76 components of the new formation rate in Beijing are discussed and compared to those from other locations in the world.

77 2 Theory

78 2.1 The new balance formula to estimate formation rate

79 The new formula based on definition of droplet current and aerosol general dynamic equation (see Appendix A for its
80 derivation) is shown in Eq. (1),

$$81 \quad I = \frac{dN_{[d_k, d_u]}}{dt} + \sum_{d_g=d_k}^{d_u-1} \sum_{d_i=d_{\min}}^{+\infty} \beta_{(i,g)} N_{[d_i, d_{i+1}]} N_{[d_g, d_{g+1}]} - \frac{1}{2} \sum_{d_g=d_{\min}}^{d_u-1} \sum_{d_i^3=\max(d_{\min}^3, d_k^3-d_{\min}^3)}^{d_{i+1}^3+d_{g+1}^3 \leq d_u^3} \beta_{(i,g)} N_{[d_i, d_{i+1}]} N_{[d_g, d_{g+1}]} + n_u \cdot GR_u \quad (1)$$

82 where J_k is the formation rate of particles at size d_k ; N is particle number concentration and $N_{[d_k, d_u]}$ is defined as total number
83 concentration of particles ranged from d_k to d_u (particles with diameters of d_u are not accounted for); d_i refers to the lower
84 bound of each measured size bin; $\beta_{(i,g)}$ is the coagulation coefficient when particles with the diameter of d_i collides with
85 particles with the diameter of d_g ; n is particle size distribution function which equals dN/dd_p ; and GR_u is particle growth rate
86 at d_u , i.e., dd_u/dt . d_u is the upper bound of the size range for calculation. d_{\min} is the size of minimum cluster in theory and the
87 lowest size limit of measuring instrument in practice. The last three terms in the right hand side (RHS) of Eq. (1) are the
88 coagulation sink term (*CoagSink*), the coagulation source term (*CoagSrc*) and the condensational growth term, respectively.

89 The two assumptions of Eq. (1) are that (a) transport, dilution, primary emission and other losses except for coagulation loss
90 in the size range from d_k to d_u are comparatively negligible; (b) when deriving the fourth term in the RHS of Eq. (1), net
91 coagulation (net result of both formation and scavenging due to coagulation) of any particle larger than d_u with other particles
92 is negligible. These two assumptions above are also the criteria to determine d_u . The mathematical expression of population
93 balance in Eq. (1) in the discrete form is illustrated by Fig. 1. Time rate of change of particles at d_k is equal to source minus
94 sink. Source are the condensational flux into d_k (J_k) and formation due to coagulation among smaller particles/clusters
95 ($CoagSrc_k$). Sink are the condensational flux out of d_k (J_{k+1}) and scavenging due to coagulation with other particles/clusters
96 ($CoagSnk_k$). Nucleation rate, I , is defined as J_k when d_k is the size of the critical cluster (nuclei). Equation (1) is obtained by
97 adding these single population balance equations up from d_k to d_u , converting it from the discrete form into the continuous
98 form, and approximating J_u with the product of measured n_u and GR_u . Note that Eq. (1) is still an approximate formula of
99 particle formation rate because $CoagSnk$ and $CoagSrc$ are calculated by size bins and the coagulation effect of particles smaller
100 than d_{min} is not accounted for. For rigorous mathematical derivation and detailed illustration, please refer to Appendix A.

101 2.2 Previous approaches to estimate formation rate

102 The population balance method proposed in previous study is shown in Eq. (2) (Kulmala et al., 2001; Kulmala et al., 2012),

$$103 J_k = \frac{dN_{[d_k, d_u]}}{dt} + CoagS_m \cdot N_{[d_k, d_u]} + \frac{N_{[d_k, d_u]}}{(d_u - d_k)} \cdot GR_{[d_k, d_u]} \quad (2)$$

104 where coagulation sink, $CoagS_m$, is defined as Eq. (3).

$$105 CoagS_m = \int_0^{+\infty} \beta_{(i,m)} n_i dd_i \quad (3)$$

106 The subscript m corresponds to the representing diameter, d_m , for particles ranged from d_k to d_u . d_m is often estimated as the
107 geometric mean diameter of d_k and d_u . Equation (1) and (2) look similar because they are both derived from the general dynamic
108 equation, while their detailed differences are illustrated in Appendix B.

109 The definition approach to calculate new particle formation rate is shown in Eq. (4) (Heisler & Friedlander, 1977; Weber et
110 al., 1996; Iida et al., 2006; Kuang et al., 2008; Kuang et al., 2012).

$$111 J_k = n_k \cdot GR_k \quad (4)$$

112 Equation (4) focuses on the flux into d_k and is theoretically correct in continuous space of particle diameter. However, when
113 applying Eq. (4) in practice, size distribution of particles smaller than d_k is required, which is difficult to obtain (See Appendix
114 B). Usually diameter bins larger than d_k are used to estimate particle formation rate when using the practical expression of Eq.
115 (4) (e.g., Eq. (9) defined in section 4.3). As illustrated in Fig. 1, such approximation essentially neglects the first three terms
116 in the RHS of Eq. (1), and may lead to underestimation of particle formation rate because of neglecting the coagulation
117 scavenging effect especially when analysing intense NPF events.

118 **2.3 Previous formulae for comparison**

119 Equation (5) is a widely used balance formula to estimate formation rate in previous studies (Kulmala et al., 2001; Dal Maso
120 et al., 2005; Wu et al., 2007; Shen et al., 2011; Wang et al., 2013),

$$121 \quad J_{1.5} = \frac{dN_{[1.5,25]}}{dt} + N_{[1.5,25]} \sum_{d_i=1.5\text{nm}}^{+\infty} \beta_{(i,8)} N_i + \frac{N_{[1.5,25]}}{(25-1.5) \text{ nm}} \cdot GR_{[1.5,25]} \quad (5)$$

122 where N_i is the number concentration of size bin i . Corresponding to those in Eq. (2), d_u is 25 nm and d_m is 8 nm in Eq. (5). By
123 comparing Eq. (5) with Eq. (1), it can be concluded that Eq. (5) estimates $CoagS_{nk}$ using a representative $CoagS_m$ and neglects
124 $CoagS_{rc}$. The growth rates in all formulae in section 2.2 were estimated using the mode-fitting method suggested in Kulmala
125 et al. (2012).

126 When calculating $CoagS_m$, particles smaller than d_m (Kulmala et al., 2012) or even d_u are neglected in some previous studies.
127 Corresponding formulae are shown in Eq. (6) and Eq. (7), respectively. The only difference among Eq. (5), Eq (6), and Eq. (7)
128 is the lower bound when calculating $CoagS_m$ in the second term in the RHS of these equations.

$$129 \quad J_{1.5} = \frac{dN_{[1.5,25]}}{dt} + N_{[1.5,25]} \sum_{d_i=8\text{nm}}^{+\infty} \beta_{(i,8)} N_i + \frac{N_{[1.5,25]}}{(25-1.5) \text{ nm}} \cdot GR_{[1.5,25]} \quad (6)$$

$$130 \quad J_{1.5} = \frac{dN_{[1.5,25]}}{dt} + N_{[1.5,25]} \sum_{d_i=25\text{nm}}^{+\infty} \beta_{(i,8)} N_i + \frac{N_{[1.5,25]}}{(25-1.5) \text{ nm}} \cdot GR_{[1.5,25]} \quad (7)$$

131 The upper bound, d_u , is selected as 6 nm in some recent studies (Sihto et al., 2006; Riipinen et al., 2007; Paasonen et al., 2009;
132 Wang et al., 2011; Vuollekoski et al., 2012; Wang et al., 2015) as shown in Eq. (8).

$$133 \quad J_{1.5} = \frac{dN_{[1.5,6]}}{dt} + N_{[1.5,6]} \sum_{d_i=1.5\text{nm}}^{+\infty} \beta_{(i,3)} N_i + \frac{N_{[1.5,6]}}{(6-1.5) \text{ nm}} \cdot GR_{[1.5,6]} \quad (8)$$

134 It should be clarified that d_k in Eq. (5)-(8) was usually 3 nm in previous studies due to the absence of sub-3 nm particle size
135 distributions, and d_m in Eq. (8) was 4 nm rather than 3 nm in previous studies because 4 nm is almost the geometrical mean
136 diameter of 3 nm and 6 nm. Particles smaller than 6 nm were neglected when estimating the coagulation sink term in some
137 studies, although its uncertainties will not be discussed here. The expression of condensational growth term, i.e., the third term
138 in the RHS of Eq. (8) varies with studies, however, it does not influence the generality of the following discussion.

139 In previous studies, several size bins larger than d_k , typically 3 nm, were adopted when using the practical formula of the
140 definition approach (Weber et al., 1996; Kuang et al., 2008), while here the size range from 1.5 nm to 2.5 nm is applied to
141 estimate $J_{1.5}$ as shown in Eq. (9).

$$142 \quad J_{1.5} = \frac{N_{[1.5,2.5]}}{(2.5-1.5) \text{ nm}} \cdot GR_{[1.5,2.5]} \quad (9)$$

143 3 Experiment

144 A NPF field campaign was carried out in Beijing. The observation period was from March 7th to April 7th, 2016. The monitoring
145 site locates on the top floor of a four-storey building in the centre of the campus of Tsinghua University. Tsinghua situates in
146 the northwestern urban area of Beijing and the fourth-ring road is ~2 km away to the south of the monitoring site. The site has
147 been a PM_{2.5} monitoring station since 1999 (He et al., 2001; Cao et al., 2014) and there are no tall buildings nearby. Potential
148 pollution sources around are the three cafeterias on campus that may produce cooking aerosol during meal time, locate ~170
149 m away on the northeast, ~170 m away on the north, and ~350 m away on the northwest, respectively.

150 A DEG-SMPS equipped with a mini- cyDMA specially designed for classification of sub-3 nm particles was deployed to
151 measure particles in the size range of 1-5 nm (Cai et al., 2017). A particle size distribution system, including a SMPS with a
152 TSI nano DMA, a SMPS with a TSI long DMA and an aerodynamic particle sizer, was used to measure particles in the size
153 range of 3 nm to 10 μm in parallel (Liu et al., 2016). Other instruments whose data are not used in this analysis are not listed
154 here.

155 A C++ program was used to invert particle size distribution from raw counts while incorporating diffusion losses inside the
156 sampling tube, diffusion losses and charging efficiencies of the bipolar neutralizers, penetration efficiencies and transfer
157 functions of DMAs, and detection efficiencies of CPCs (Hagen and Alofs, 1983; Jiang et al., 2011a). The particle density was
158 assumed to be 1.6 g/cm³ according to local observation results (Hu et al., 2012). Mass accommodation coefficient was assumed
159 to be unity and temperature was assumed to be a constant value of 285 K, the average temperature during the observation
160 period.

161 4 Results and discussion

162 4.1 Upper size bound for formation rate calculation

163 New particle formation rates using different upper size bound, d_u of 3 nm, 6 nm, 10 nm and 25 nm were calculated. Since the
164 maximum size that new particles formed by nucleation have reached varies with time, the upper size bound should not be a
165 constant value to minimize the interference of background particles. A varying upper size bound, d_b , was visually determined
166 as the largest size bin in the size range from 3 nm to 25 nm whose frequency density (particle size distribution), $dN/d\log d_p$,
167 was larger than 28,000 #/cm³. Here 28,000 was determined visually according to the measured intensity plot of particle size
168 distributions as an approximate boundary for newly formed particles and background particles. The value should be campaign
169 specific or even event specific. Fig. 2(a) indicates that d_b is almost the boundary for particles formed due to nucleation.
170 Estimated $J_{1.5}$ using 20,000 #/cm³ as the boundary differed little from that using 28,000 #/cm³, indicating the estimated $J_{1.5}$ is
171 insensitive to the value for boundary. It is reasonable to regard d_b as a relatively credible value when compared to others. Note

172 that when using d_b as the upper size bound, dN/dt term of newly formed particles in Eq. (1) is approximated by that of sub-25
173 nm particles to avoid potential influence of varying size range on particle number concentration.

174 As shown in Fig 2(b), estimated $J_{1.5}$ using d_b and a constant value of 25 nm as the upper bounds are almost the same (the mean
175 relative error is 2.2%). The maximum difference between these two choices is ~10% which appears before 8:00 when d_b is
176 less than 5 nm and the number concentration of sub-25 nm particles is ~2 times of sub-6 nm particles and ~3 times of sub-3
177 nm particles. This indicates that the influence of non-freshly nucleated particles on estimating $J_{1.5}$ is not important because
178 their comparatively low diffusivities even though their concentration is comparatively high at the beginning of NPF events.
179 Estimated $J_{1.5}$ using d_u of 6 nm and 10 nm are in good consistency with that using d_b before 10:00 (the mean relative errors are
180 4.8% and 2.6%, respectively). However, when particles formed by nucleation grow beyond the upper size bound, calculated
181 $J_{1.5}$ is underestimated when using 6 nm and 10 nm as the upper bound. For example, the mean relative errors of estimated $J_{1.5}$
182 using d_u of 6 nm and 10 nm between 10:30 and 15:00 are 18.6% and 12.8%, respectively. When calculating $J_{1.5}$ using 3 nm as
183 d_u , an average 47% underestimation was found for this event.

184 The reason for underestimation when using smaller d_u can be illustrated by Fig. 2(c). J_u is estimated by $n_u \cdot GR_u$ in Eq. (1).
185 This estimation may be not accurate when d_u is small because the assumption that net coagulation of any particle larger than
186 d_u with other particles is negligible may be violated. As illustrated in the derivation of Eq. (1) in Appendix A, a nearly zero J_u
187 is preferred when using Eq. (1). However, as shown in Fig 2(c), estimated J_3 is still a large fraction compared to $J_{1.5}$, while J_6
188 and J_{10} are 27.8% and 17.6% of $J_{1.5}$ on average between 10:30 and 15:00, respectively. Although J_u is approximated by
189 $n_u \cdot GR_u$ rather than simply neglected, this approximation may still lead to uncertainties.

190 Since $J_{1.5}$ estimated by the varying d_b and a constant value of 25 nm are almost the same with an acceptable relative error even
191 under the interference of non-freshly nucleated particles, 25 nm was adopted as the upper bound for calculating J in this study.
192 It is reasonable to neglect J_u for simplicity when d_u is determined according to the two criteria. It should be clarified that 25
193 nm is not necessarily valid for all other studies, because the upper bound should be determined by the two criteria and can be
194 campaign specific. However, it can be concluded that a very small upper bound, such as 3 nm is not recommended because
195 particles formed by nucleation surely grow larger than 3 nm in a typical NPF event while intense primary emission of particles
196 around 3 nm is rarely observed in the atmosphere (unless near the emission sources).

197 **4.2 Comparison with previous formulae**

198 Estimated $J_{1.5}$ values using Eq. (1) and Eq. (5)-(9) on March 13th are shown in Fig. 3. d_k , d_u , and d_{min} are 1.5 nm, 25 nm, and
199 1.3 nm, respectively, when using Eq. (1). It can be concluded that except for Eq. (8), other formulae significantly underestimate
200 $J_{1.5}$ compared to Eq. (1). By comparing contribution of each terms in the RHS of Eq. (1) and Eq. (5)-(9), it was found that the
201 underestimation of formation rates is mainly caused by the underestimation of *CoagSnk*. Equation (9) simply neglects *CoagSnk*

202 as well as other terms (dN/dt and $CoagSrc$) compared to Eq. (1), so its result is the lowest among six formulae. Equation (5)
203 estimates $CoagSnk$ using an average $CoagS_m$, which lead to underestimation because $CoagS$ at 8 nm happens to be smaller
204 than those at most other diameters in the size range from 1.5 nm to 25 nm, as illustrated in Appendix B. Equation (6) and (7)
205 neglects particles smaller than 8 nm and 25 nm when calculating $CoagS_m$, respectively. Such simplification may be reasonable
206 for relative clean atmosphere where nucleation intensity is not strong, however, these approximations are not suitable for
207 analysing typical NPF events in Beijing where coagulation among nucleation mode particles is a major proportion of $CoagSnk$.
208 $J_{1.5}$ estimated using Eq. (8) agrees well with that estimated using Eq. (1), however, it does not mean that 6 nm serve as a better
209 upper size bound than 25 nm. The agreement between results estimated using Eq. (1) and (8) is due to both the more accurate
210 estimation of $CoagSnk$ when using an average $CoagS_m$ in a narrower size range. In addition, in this case the underestimation
211 of $CoagSnk$ when using Eq. (8) is coincidentally cancelled out by the overestimation of formation rate caused by neglecting
212 $CoagSrc$.

213 The importance of coagulation scavenging among newly formed particles due to nucleation is illustrated in Fig. 4. Scavenging
214 due to coagulation with particles smaller than d_p is neglected, as mathematically defined in the formula in Fig. 4(a). $CoagSnk$
215 increases rapidly with the decrease in d_p rather than maintain an approximately constant value during NPF events, indicating
216 coagulation among nucleated particles contribute a considerable fraction to $CoagSnk$ in Beijing. The necessity of sub-3 nm
217 particle size distribution is also demonstrated, which means estimated J_3 may also be underestimated due to the absence of
218 sub-3 nm data, as illustrated in Appendix B. Approximation of $CoagSnk$ estimated using a representative $CoagS_m$ is also shown
219 in Fig. 4(b), indicating the underestimation of new particle formation rate when applying Eq. (5) to analyse NPF events in
220 Beijing. However, calculated $CoagSnk$ on a non-NPF event day as well as at non-NPF periods on NPF day is almost unaffected
221 by the coagulation scavenging effect of particles in nucleation mode (smaller than 25 nm), because number concentration of
222 nucleation mode particles at non-NPF time is comparatively low.

223 **4.3 Characteristics of estimated formation rate in Beijing**

224 For the NPF events observed in the Beijing campaign, $CoagSnk$ is a governing component of the estimated $J_{1.5}$. The estimated
225 formation rate on March 13th and the four terms in the RHS of Eq. (1), i.e., dN/dt , $CoagSnk$, $CoagSrc$, and the condensational
226 growth term, are shown in Fig. 5. $CoagSnk$ is almost the same with the estimated $J_{1.5}$ in Beijing, while the difference between
227 them is mainly due to dN/dt whose absolute value is comparatively higher at the beginning and the end of the NPF event. The
228 condensational growth term, $n_u \cdot GR_u$, is negligible compared to other terms, which is reasonable since J_u is supposed to be
229 unimportant when determining d_u in Eq. (1). The governing role of $CoagSnk$ in estimated formation rate in Beijing emphasizes
230 the importance of fully considering the coagulation scavenging effect among particles formed by nucleation. Equation (5)-(9)
231 may fit well in relatively clean atmospheric environment where new particle formation rate is comparatively low, such as in

232 Hyytiälä, and agreement of Eq. (8) and Eq. (9) has been reported in a numerically simulated NPF event in which J_3 is less than
233 $1 \text{ cm}^{-3}\text{s}^{-1}$ (Vuollekoski et al., 2012). However, problems appear when applying them in urban Beijing because of
234 underestimating the governing fraction of estimated $J_{1.5}$, i.e., $CoagSnk$.

235 Coagulation sink, $CoagS$, is not the major reason for the governing role of $CoagSnk$ in Beijing. It is generally considered that
236 the atmosphere in typical urban area in China, such as Beijing, is comparatively polluted. However, observed NPF events
237 mainly occurs on clean days when the air mass comes from north or northwest of Beijing. The mean $PM_{2.5}$ mass concentration
238 reported by the nearest national monitoring station, Wanliu station, was $10.4 \mu\text{g}/\text{cm}^3$ during all NPF events in this campaign.
239 The aerosol surface area concentration is characterized by Fuchs surface area, A_{Fuchs} (McMurry, 1983), and condensation sink,
240 CS (Kulmala et al., 2001), which are often used to examine the coagulation scavenging effect. The positive correlation between
241 A_{Fuchs} and CS is illustrated in McMurry et al. (2005), while CS can be regarded as the $CoagS$ of sulphuric acid molecules. Fig.
242 6(a) shows the comparison of A_{Fuchs} and CS in Beijing to those in other locations around the world. A_{Fuchs} and CS during NPF
243 events in this study are higher than those in Hyytiälä, similar to those observed in Boulder, and lower than those in Atlanta,
244 Mexico City, and New Delhi. This indicates that coagulation sink in urban Beijing on NPF days is in common range rather
245 than higher than most other places around the world.

246 As shown in Equation (1), $CoagSnk$ is approximately proportional to the square of particle number concentration. Nucleation
247 intensity in urban Beijing, characterized by number concentration of particles larger than 3 nm during typical NPF event
248 periods, is found to be higher than those in Hyytiälä and Atlanta (as shown in Fig. 6(b)). Number concentration of sub-3 nm
249 particles is not accounted for to maintain comparability. Although A_{fuchs} and $CoagS$ represent the relative importance of the
250 coagulation scavenging effect (McMurry, 1983; Kulmala et al., 2001), it is the $CoagSnk$ that reflects the number of particles
251 lost due to coagulation scavenging in the size range of d_k to d_n . This explains the governing status of $CoagSnk$ in estimated
252 formation rates in urban Beijing with intense NPF events.

253 Fig. 7 further illustrate the underestimation in new particle formation rates in China due to previously used formulae, especially
254 for Eq. (7) which neglects coagulation among sub-25 nm particles and Eq. (9) which simply neglects net coagulation effect.
255 The mean $J_{1.5}$ estimated in this study using Eq. (1) are 1.2, 2.4, and 6.4 times those estimated using Eq. (5), Eq. (7), and Eq.
256 (9), respectively. The mean J_3 estimated in this study using Eq. (1) are 1.2, 2.0, and 3.3 times those estimated using Eq. (5),
257 Eq. (7), and Eq. (9), respectively. J_3 reported in previous studies in urban Beijing (Wu et al., 2007; Yue et al., 2009; Wang et
258 al., 2013; Wang et al., 2015), Shanghai (Xiao et al., 2015) and Shangdianzi, the regional background station of North China
259 Plain (Shen et al., 2011; Wang et al., 2013), are also shown in Fig. 7. Higher formation rates are anticipated if the coagulation
260 scavenging effect are fully considered when analysing these NPF events. Note that sub-3 nm particles is also accounted when
261 calculating J_3 in this study, while not in previous ones except for the campaign in Shanghai.

262 4 Conclusions

263 A new balance formula to estimate new particle formation rate derived from aerosol general dynamic equation was proposed.
264 The new formula estimates the effect of coagulation scavenging better compared to previously used ones. Two criteria in
265 determining the upper bound for calculation were proposed. A NPF campaign in urban Beijing was carried out in spring of
266 2016. Aerosol size distributions down to ~1 nm was measured and used to test the new formula and those widely used ones in
267 previous studies. It was found that formation rates in urban Beijing are underestimated to different extents in previously used
268 formulae, and the underestimation of the coagulation scavenging effect (corresponding to the coagulation sink term) is the
269 major reason. Coagulation among particles in nucleation mode was found to be important when estimating the coagulation
270 scavenging effect in urban Beijing. The estimated formation rates of 1.5 nm particles in this campaign using the new formula
271 were 1.3 – 4.3 times those estimated using the formula neglecting coagulation among particles in the nucleation mode. The
272 coagulation sink term is the governing component of the estimated formation rate in urban Beijing. Although higher than those
273 in relative clean atmosphere, such as in Hyytiälä, coagulation sink (expressed in the form of Fuchs surface area and
274 condensation sink) in urban Beijing on NPF days is lower than those reported in Atlanta and Mexico City. However, the
275 number concentration of particles formed due to nucleation in urban Beijing is comparatively high, which lead to high
276 coagulation loss. The formulae used in previous studies may perform well when describing relative weak NPF events in clean
277 atmosphere, while they underestimate the coagulation scavenging effect when analysing intense NPF events. Formation rates
278 reported in previous studies for urban Beijing and other locations with intense NPF events might be underestimated because
279 of their underestimation or neglect of the coagulation scavenging effect.

280 Appendix A

281 Derivation of nucleation rate from aerosol general dynamic equation

282 Nucleation rate is the rate at which particles grow past the size of the critical cluster (nuclei). However, a more specific and
283 microscopic definition of nucleation rate is needed for any further calculation, and it should be easily and unambiguously
284 transferred into a mathematical expression. Here we adopt the definition based on droplet current (Eq. 10.1, Friedlander, 2000):

$$285 J_g = \beta_{(1,g-1)} N_1 N_{g-1} - \alpha_g s_g N_g . \quad (A1)$$

286 Formation rate, J_g , is the excess rate of the passage from g-1 (cluster or particle with g-1 molecules) to g by condensation over
287 the passage from g to g-1 by evaporation. If g is the size of the critical cluster, J_g is defined as nucleation rate, I . N_g is the
288 number concentration of cluster g; $\beta_{(i,j)}$ is the coagulation coefficient of i and j, and it can be theoretically estimated by diameter
289 of i and j (Eq. 13.56, Seinfeld & Pandis 2006); α_g is the monomer evaporation flux from g; and s_g is the effective surface area
290 of g for evaporation. Only formation due to condensational growth is considered in the definition of Eq. (A1), while formation

291 due to coagulation of smaller clusters is not taken into account. This is based on the assumption that critical clusters are mainly
 292 formed due to condensational growth of sulfuric acid and other chemical species. The formation of critical cluster by
 293 coagulation does not influence the generality of the following derivation and can be readily incorporated, and it will be clarified
 294 at the end of Appendix A.

295 The other basic equation for the derivation is the general dynamic equation in the discrete form (Eq. 11.3, Friedlander 2000),

$$296 \frac{dN_g}{dt} = \frac{1}{2} \sum_{\substack{i+j=g \\ i,j \geq 2}} \beta_{(i,j)} N_i N_j - \sum_{i=2}^{+\infty} \beta_{(i,g)} N_i N_g + \beta_{(1,g-1)} N_1 N_{g-1} - \beta_{(1,g)} N_1 N_g - \alpha_g s_g N_g + \alpha_{g+1} s_{g+1} N_{g+1}. \quad (\text{A2})$$

297 As shown in Eq. (A2), time rate of change of cluster or particle number concentration, dN_g/dt in the left-hand side (LHS), is
 298 determined by formation due to coagulation of smaller clusters and (or) particles, coagulation scavenging with pre-existing
 299 clusters and particles, condensational growth from $g-1$ and to $g+1$, and evaporation to $g-1$ and from $g+1$, corresponding to the
 300 six terms in the right-hand side (RHS) of Eq. (A2), respectively. The evaporation terms (corresponding to the fifth and sixth
 301 terms in the RHS) may be zero or nearly zero when g is large, however, their exact values have no influence on derivation. An
 302 important assumption to be noted is that meteorological transport, dilution, primary emission of g and other losses (e.g., wall
 303 loss) are not included in Eq. (A2).

304 Notice that the last four terms in the RHS of Eq. (A2) are equal to $J_g - J_{g+1}$ by substituting Eq. (A1) in. Replacing subscript g
 305 with the critical cluster size, k , we have:

$$306 I := J_k = \frac{dN_k}{dt} + \sum_{i=2}^{+\infty} \beta_{(i,k)} N_i N_k - \frac{1}{2} \sum_{\substack{i+j=k \\ i,j \geq 2}} \beta_{(i,j)} N_i N_j + J_{k+1}. \quad (\text{A3})$$

307 The expression of Eq. (A3) is similar to Eq. (A6) in Kuang et al. (2012), which was also obtained using the balance method.
 308 J_{k+1} is usually a relatively large term in Eq. (A3), and it can be accounted for by iteration. Equation (A5) is obtained by
 309 summing Eq. (A3) up from subscript k to $u-1$ as shown in Eq. (A4), where u is the particle size at the upper bound of the
 310 concerned size range.

$$311 \begin{aligned} I - J_{k+1} &= \frac{dN_k}{dt} + \sum_{i=2}^{+\infty} \beta_{(i,k)} N_i N_k - \frac{1}{2} \sum_{\substack{i+j=k \\ i,j \geq 2}} \beta_{(i,j)} N_i N_j \\ J_{k+1} - J_{k+2} &= \frac{dN_{k+1}}{dt} + \sum_{i=2}^{+\infty} \beta_{(i,k+1)} N_i N_{k+1} - \frac{1}{2} \sum_{\substack{i+j=k+1 \\ i,j \geq 2}} \beta_{(i,j)} N_i N_j \\ &\dots = \dots \end{aligned} \quad (\text{A4})$$

$$312 \begin{aligned} J_{u-1} - J_u &= \frac{dN_{u-1}}{dt} + \sum_{i=2}^{+\infty} \beta_{(i,u-1)} N_i N_{u-1} - \frac{1}{2} \sum_{\substack{i+j=u-1 \\ i,j \geq 2}} \beta_{(i,j)} N_i N_j \\ I &= \frac{d \sum_{g=k}^{u-1} N_g}{dt} + \sum_{g=k}^{u-1} \sum_{i=2}^{+\infty} \beta_{(i,g)} N_i N_g - \frac{1}{2} \sum_{g=k}^{u-1} \sum_{\substack{i+j=g \\ i,j \geq 2}} \beta_{(i,j)} N_i N_j + J_u \end{aligned} \quad (\text{A5})$$

313 In the RHS of Eq. (A5) are the time rate of change of the particle concentration, the coagulation sink term, the coagulation
 314 source term and the condensational growth term, respectively. Note that when particle u is large enough, J_u is nearly zero, i.e.,
 315 $\lim_{u \rightarrow \infty} J_u = 0$, because of their negligible condensational growth and low number concentration compared to those of freshly
 316 nucleated small particles. Equation (A6) is obtained by replacing the upper bound, u , with infinite and further simplified by
 317 combining the second and third term in the RHS of Eq. (A5).

$$318 \quad I = \frac{d \sum_{g=k}^{+\infty} N_g}{dt} + \frac{1}{2} \sum_{g=k}^{+\infty} \sum_{i=k}^{+\infty} \beta_{(i,g)} N_i N_g \quad (A6)$$

319 Theoretically, Eq. (A6) can be used to estimate I since each term in the RHS can be calculated. However, the validity of Eq.
 320 (A6) faces higher risk of violation when applied in real atmosphere due to non-negligible primary emission sources, since Eq.
 321 (A6) is a balance equation for the whole aerosol population rather than a limited size range of the nucleation mode. It's both
 322 more cautious and efficient to use Eq. (A5) with a proper particle size u and a reasonable estimation of J_u .

323 When using measured particle size distribution to estimate I , Eq. (A5) has to be converted from the discrete form into the
 324 continuous form. For the third term in the RHS of Eq. (A5), i.e., the coagulation source term, its summation sequence can be
 325 rearranged as,

$$\begin{aligned} & \frac{1}{2} \sum_{g=k}^{u-1} \sum_{\substack{i+j=g \\ i,j \geq 2}} \beta_{(i,j)} N_i N_j \\ &= \frac{1}{2} \beta_{(2,k-2)} N_2 N_{k-2} + \dots + \frac{1}{2} \beta_{(k-2,2)} N_{k-2} N_2 \\ 326 &+ \dots \\ &+ \frac{1}{2} \beta_{(2,u-3)} N_2 N_{u-3} + \dots + \frac{1}{2} \beta_{(k-2,u-k+1)} N_{k-2} N_{u-k+1} + \dots + \frac{1}{2} \beta_{(u-3,2)} N_{u-3} N_2 \\ &= \frac{1}{2} \sum_{g=2}^{u-3} \sum_{i=\max(2,k-g)}^{i+g \leq u-1} \beta_{(i,g)} N_i N_g \end{aligned} \quad (A7)$$

327 The formulae in both the far LHS and the far RHS of Eq. (A7) are equally accurate to estimate the coagulation source term.
 328 However, simply substituting the continuous particle diameter (e.g., d_g) for the discrete size (e.g., g) in the far LHS of Eq. (A7)
 329 will result in uncertainties when the size bins do not increase linearly in the particle volume space. As indicated in Fig. A1,
 330 substituting the continuous particle diameter for the discrete size in the far RHS of Eq. (A7) is independent of the bin structure
 331 for d_g and d_i .

332 Thus, Eq. (A5) can be rewritten as,

$$333 \quad I = \frac{dN_{[d_k, d_u]}}{dt} + \sum_{d_g=d_k}^{d_{u-1}} \sum_{d_i=d_{min}}^{+\infty} \beta_{(i,g)} N_{[d_i, d_{i+1}]} N_{[d_g, d_{g+1}]} - \frac{1}{2} \sum_{d_g=d_{min}}^{d_{u-1}} \sum_{d_i^3=\max(d_{min}^3, d_k^3-d_{min}^3)}^{d_{i+1}^3+d_{g+1}^3 \leq d_u^3} \beta_{(i,g)} N_{[d_i, d_{i+1}]} N_{[d_g, d_{g+1}]} + J_u \quad (A8)$$

334 where d_{min} is theoretically the minimum cluster size. Note that the size bin from d_{u-1} to d_u is denoted by subscript $u-1$, so the
 335 upper bound of the size range for calculation is d_u . The discrete upper sizes, $u-1$ in Eq. (A5) and $u-3$ in Eq. (A7), are
 336 approximated by d_u in Eq. (A8). $N_{[d_k, d_u]}$ is defined as the number concentration in the size range from d_k to d_u (particles with

337 diameters of d_u are not accounted for), corresponding to $\sum_{g=k}^{u-1} N_g$ in the discrete form. Since measured size bins are finite, Eq.
338 (A8) is expressed in the summation form rather than the integration form. Practically, Eq. (A8) is only an estimation of Eq.
339 (A5) because coagulation is calculated by size bins, while particles sizes in each size bin are not exactly the same as the
340 representing diameter, d_g . The upper size bound, d_u , is a “properly large” size at which diameter J_u is negligible compared to
341 the sum of the others three terms in the RHS of Eq. (A8). “Properly large” is defined by the following two criteria: the one is
342 d_u shouldn’t be too large so that the calculated nucleation rate is non-negligibly affected by transport or primary emissions; the
343 other is d_u shouldn’t be too small so that the calculated nucleation rate is underestimated because J_u is still too large to be
344 neglected or to be estimated by growth rate (as illustrated in the following paragraph). These two criteria seem to be
345 contradictory, however, as illustrated in Fig. 2b, calculated nucleation rate is usually not sensitive to the upper bound because
346 J_u decreases rapidly with the increase of d_u since the freshly nucleated particles are usually in a relatively narrow size range,
347 especially during strong NPF events.

348 The fourth term in the RHS of Eq. (A8), J_u , is usually so small that it can be simply neglected when d_u is “properly large”.
349 However, an approximate term is recommended for better estimation. Here we introduce a sufficient but possibly unnecessary
350 condition that net coagulation effect between any particle larger than d_u and other particles can be neglected. Define
351 $N_{[d_u, d_u + \Delta d]}|_t$ as number concentration of particles in a narrow size range from d_u to $d_u + \Delta d$ at time t. After a very short time dt ,
352 these particles grow into the size range from $d_u + dd$ to $d_u + \Delta d + dd$, which is based on the assumption that diameter growth is
353 equal for different particles in such narrow size and time range, while number concentration remains the same since there is
354 no particle loss. Particles in the size range from $d_u + \Delta d$ to $+\infty$ at time t grow up to the size range from $d_u + \Delta d + dd$ to $+\infty$,
355 correspondingly. And since the size range is narrow enough, it’s reasonable to assume that concentration of particles is equally
356 distributed in the size range from d_u to $d_u + \Delta d + dd$, i.e.,

$$357 \frac{N_{[d_i, d_j]}|_{t+dt}}{N_{[d_m, d_n]}|_{t+dt}} = \frac{d_j - d_i}{d_n - d_m}, \text{ for any } d_i, d_j, d_m, d_n \in [d_u, d_u + \Delta d + dd]. \quad (\text{A9})$$

358 Particle size distribution function, n , and growth rate, GR , are defined as Eq. (A10) and (A11), respectively. Equation (A12)
359 is obtained by combining Eq. (A6), Eq. (A9), Eq. (A10), and Eq. (A11).

$$360 n_u = \frac{dN}{dd} \Big|_{d_u} = \lim_{\Delta d \rightarrow 0} \frac{N_{[d_u, d_u + \Delta d]}}{\Delta d} \quad (\text{A10})$$

$$361 GR_u = \frac{dd}{dt} \Big|_{d_u} \quad (\text{A11})$$

$$362 J_u = \frac{dN_{[d_u, +\infty]}}{dt} = \frac{N_{[d_u, d_u + dd]}|_{t+dt} + N_{[d_u + dd, +\infty]}|_{t+dt} - N_{[d_u, +\infty]}|_t}{dt}$$

$$\begin{aligned}
363 \quad &= \frac{N_{[d_u, d_u+dd]} \Big|_{t+dt}}{dt} \\
364 \quad &= \lim_{\Delta d \rightarrow 0} \frac{N_{[d_u, d_u+dd]} \Big|_{t+dt}}{N_{[d_u+dd, d_u+\Delta d+dd]} \Big|_{t+dt}} \cdot N_{[d_u+dd, d_u+\Delta d+dd]} \Big|_{t+dt} \cdot dt \\
&= \lim_{\Delta d \rightarrow 0} \frac{dd}{\Delta d \cdot dt} \cdot N_{[d_u, d_u+\Delta d]} \Big|_t \\
365 \quad &= n_u \cdot GR_u \tag{A12}
\end{aligned}$$

366 Finally combining Eq. (A8) and Eq. (A12) we can obtain the equation to estimate nucleation rate as Eq. (A13),

$$367 \quad I = \frac{dN_{[d_k, d_u]}}{dt} + \sum_{d_g=d_k}^{d_u-1} \sum_{d_i=d_{min}}^{+\infty} \beta_{(i,g)} N_{[d_i, d_{i+1}]} N_{[d_g, d_{g+1}]} - \frac{1}{2} \sum_{d_g=d_{min}}^{d_u-1} \sum_{d_i^3=\max(d_{min}^3, d_k^3-d_{min}^3)}^{d_{i+1}^3+d_{g+1}^3 \leq d_u^3} \beta_{(i,g)} N_{[d_i, d_{i+1}]} N_{[d_g, d_{g+1}]} + n_u \cdot GR_u. \tag{A13}$$

368 The first term in the RHS of Eq. (A13) is the change in the number concentration of particles ranged from d_k to d_u . The second
369 and third terms are particle loss to coagulation scavenging and particle formation by coagulation, named as the coagulation
370 sink term (*CoagSnk*) and the coagulation source term (*CoagSrc*), respectively (Kuang et al, 2012). The fourth term is the
371 condensational growth term, which is an approximation of the formation rate, J_u . This balance formula derived from aerosol
372 general dynamic equation can also be expressed as Eq. (A14).

$$373 \quad I = \frac{dN_{[d_k, d_u]}}{dt} + CoagSnk - CoagSrc + n_u \cdot GR_u \tag{A14}$$

374 When applying Eq. (A13) in practice, d_k is usually the assumed size of the critical nuclei (or the lowest size limit of instrument,
375 corresponding to formation rate, J_k , rather than nucleation rate, I). The dN/dt term can be obtained either by differentiating
376 between adjacent time bins or fitting in a continuous time period. *CoagSnk* and *CoagSrc* can be directly calculated from particle
377 size distribution, where d_{min} is the minimum detected particle diameter. If formation by coagulation of smaller clusters is also
378 included in the definition of nucleation rate, calculation of *CoagSrc* (the third term in the RHS of equation A(12)) should begin
379 with d_{k+1} instead of d_k , which usually affects little since the difference is only a size bin and the whole *CoagSrc* is usually a
380 minor term of J in atmosphere environment. Growth rate can be estimated by different methods (Weber et al., 1996; Weber et
381 al., 1997; Kulmala et al., 2012; Lehtipalo et al., 2014), or the growth term can be simply neglect when d_u is “properly large”.
382 It should be clarified that the formation rate calculated using Eq. (A13) may be underestimated because coagulation scavenging
383 by particles and clusters smaller than d_{min} is neglected due to the limitation of measuring instruments. As illustrated in Fig.
384 6(a), *CoagSnk* calculated using d_p larger than 3 nm is ~ 89.1% of that using d_p larger than 1.5 nm. It could be inferred that the
385 calculated J_3 was slightly underestimated in some previous studies lacking size distribution for sub-3 nm particles. While in
386 this study, measured particles down to 1.3 nm are accounted for when calculating $J_{1.5}$ and J_3 . Neglecting coagulation between
387 clusters may also have a non-negligible effect on the calculated results (McMurry 1983), which calls for measurement of major
388 molecular clusters participating in nucleation if more accurate formation rate is to be obtained.

390 **Relationships with previous approaches**

391 Since the new balance approach proposed in this study is based on aerosol general dynamic equation with a reasonable
 392 assumption that net coagulation of any particle larger than the “properly large” upper bound, d_u , and other particles can be
 393 neglected, its inner relationships with former approaches can be elucidated by making additional assumptions and
 394 approximations.

395 Formation rate is defined as the flux that particles grow pass through the given size, and can be expressed as Eq. (B1), where
 396 k is the number of molecules contained by the particle (Heisler & Friedlander, 1977; Weber et al., 1996; Kuang et al., 2008;
 397 Kuang et al., 2012). Note that Eq. (B1) is valid only when it is in the continuous space of particle diameter, while a more
 398 accurate expression in the discrete form is shown as Eq. (B2).

$$399 \quad J_k = n_k \cdot GR_k \quad (B1)$$

$$400 \quad J_k = n_{k-1} \cdot GR_{k-1} \quad (B2)$$

401 Eq. (B2) is believed to be theoretically correct since the only condensational flux into d_k is the growth of smaller clusters or
 402 particles with diameter of d_{k-1} . Although in similar expression with Eq. (A12), Eq. (B2) focuses on the flux into rather than out
 403 of the size bin for calculation, and there's no need to account for coagulation scavenging, as illustrated in Fig. 1.

404 A theoretical expression of GR proposed in previous study is shown as Eq. (B3), where α is herein the coagulation efficiency
 405 (fraction of collisions that successfully result in coagulation), V_1 is the volume increment when adding a single gaseous
 406 precursor, and v is the mean thermal velocity of the gaseous precursor (Weber et al., 1996). Here we update the equation by
 407 considering different chemical species and describing coagulation by β , as shown in Eq. (B4). The subscript c denotes different
 408 chemical species of monomers participating in the condensational growth of cluster $k-1$, and N_{1c} is their corresponding number
 409 concentration. Coagulation efficiency is included in each $\beta_{(1c,k)}$ (Eq. 13.56, Seinfeld & Pandis 2006).

$$410 \quad GR_k = \frac{\alpha V_1 N_1 v}{2} \quad (B3)$$

$$411 \quad GR_{k-1} = \frac{\sum_c \beta_{(1c,k-1)} N_{1c} N_{k-1}}{n_{k-1}} \quad (B4)$$

412 Eq. (B2) is theoretically correct, however, it faces difficulties when applying in practice, since n_{k-1} is obtained by approximation
 413 over some size range around d_k rather than the true frequency density at cluster $k-1$, dN_{k-1}/dd_{k-1} . Moreover, because size
 414 distribution smaller than d_k is difficult to obtain, the size range for estimation is usually larger than d_k . For example, the formula
 415 to estimate J_3 using nano-SMPS data in Kuang et al. (2008) is shown as Eq. (B5). Although Eq. (B5) seems to be an estimation
 416 of Eq. (B2), they are essentially two different equations. This is because the measured particle number concentration in the
 417 size range for calculation, i.e., N_{3-6} in Eq. (B5), has been affected by coagulation. By comparing with Eq. (A14), it can be

418 concluded that dN/dt , $CoagS_{nk}$ and $CoagS_{src}$ are simply neglected in Eq. (B5), while Eq.(B2) does not suffer from this problem
 419 by its definition.

$$420 \quad J_3 \approx \frac{N_{3-6}}{3 \text{ nm}} \cdot GR_{1-3} \quad (\text{B5})$$

421 There are also problems in estimating GR_{k-1} . Equation (B4) is only a theoretical formula, since it is nearly impossible to
 422 determine all the chemical species contributing to nucleation and their corresponding coagulation coefficients in the
 423 complicated atmospheric environment. GR calculated by sulfuric acid itself using Eq. (B3) may lead to underestimation (Kuang
 424 et al., 2010), while uncertainties also exist in the approaches which fit particles size distribution to obtain GR (Kulmala et al.,
 425 2012; Lehtipalo et al., 2014) because the effect of coagulation on measured size distribution is also neglected. So conclusively,
 426 Eq. (B2) is considered to be theoretically correct, however, it's not recommend to be applied for analyzing NPF events with
 427 high coagulation scavenging.

428 The other approach is a balance method based on a macroscopic point of view shown as Eq. (B6) (Kulmala et al., 2001;
 429 Kulmala et al., 2004), and here we adopt the equation in the most recent paper (Kulmala et al, 2012). Usually d_m is the geometric
 430 mean diameter of d_k and d_u . However, coagulation between any particle smaller than d_m or even d_u with another particle (with
 431 any size) is sometimes neglected when it comes to calculation, such as the formula suggested in Kulmala et al (2012) shown
 432 as Eq. (B7).

$$433 \quad J_k = \frac{dN_{[d_k, d_u]}}{dt} + CoagS'_m \cdot N_{[d_k, d_u]} + \frac{N_{[d_k, d_u]}}{(d_u - d_k)} \cdot GR_{[d_k, d_u]} \quad (\text{B6})$$

$$434 \quad CoagS'_m = \sum_{d_i=d_m}^{+\infty} \beta_{(i,m)} N_i \quad (\text{B7})$$

435 Eq. (B6) appears similar to Eq. (A14) since they both originate from the population balance method, however, there are some
 436 differences between them.

437 Firstly, the upper bound of particle size in Eq. (B6), d_u , is lack of strict definition and discussion. As discussed in Appendix A,
 438 d_u should be decided by the two criteria that effects of transport and primary emission are negligible and the condensational
 439 growth term, J_u , is relative small compared to J_k . The upper bound of 25 nm is usually reasonable since high concentration of
 440 particle formed by nucleation predominates the coagulation sink term during strong new particle formation time, while the
 441 upper bound of 6 nm may lead to underestimation when freshly formed particles grow beyond, as discussed in the main text.

442 Secondly, scavenging by coagulation with particles smaller than d_m is not included if using Eq. (B7) to calculate $CoagS$. As
 443 shown in Fig. B1, $CoagS$ is always larger than $CoagS'$, and their difference increases as d_m increases. $CoagS'_{8nm}$ is ~31% of
 444 $CoagS_{8nm}$, indicating a large amount of underestimation when using Eq. (B7). Note that Eq. (3) and the approximation formula
 445 (estimated with condensation sink) proposed by Lehtinen et al. (2007) does not suffer from this problem.

446 Thirdly, the second term in the RHS of Eq. (B6) is not always a reasonable approximation of $CoagS_{nk}$ in Eq. (A13) and Eq.
 447 (A14). Theoretically, the relationship between $CoagS_{nk}$ and $CoagS$ is shown as Eq. (B8), while $CoagS_m$ is chosen as the
 448 representative value when estimating J using Eq. (B6).

$$449 \quad CoagS_{nk} = \sum_{d_g=d_k}^{d_u} CoagS_g \cdot N_g \quad (B8)$$

450 However, neither is $CoagS$ a relatively constant value versus particle diameter nor is $CoagS_m$ the mean value of $CoagS$ in
 451 calculated size range from d_k to d_u . As illustrated in Fig. B1, coagulation coefficient with 8 nm particles decreases rapidly with
 452 the increase in d_i when particle is smaller than 8 nm. The minimum value of $\beta_{(d_i, 8nm)}$ appears at d_i around 8 nm because
 453 particles with similar thermal velocities are more difficult to collide with each other. The calculated $CoagS'$ during a strong
 454 NPF event on Mar. 27th, 2016 appears monotonously decreasing with the increase of d_m , while the calculated $CoagS$ has a
 455 minimum value at 6.7 nm because $CoagS$ is mainly attributed to nucleation mode particles during NPF events. In this example,
 456 $CoagS_{8nm}$ and $CoagS'_{8nm}$ are ~22.6% and ~7.2% of $CoagS_{1.5nm}$, respectively, indicating non-negligible underestimation of the
 457 coagulation sink term as well as nucleation rate when using a constant $CoagS_m$ instead of a varying value (as a function of
 458 particle diameter).

459 Fourthly, particle formation by coagulation is neglected in Eq. (B6). The absence of $CoagSrc$ will lead to an overestimation of
 460 nucleation rate. However, it sometimes coincidentally cancels out with the underestimation caused by using $CoagS_m$ to
 461 approximate $CoagSrc$, as discussed in the main text.

462 Fifthly, the growth term in Eq. (B6) is estimated over the whole size range from d_k to d_u , while in Eq. (A13) it is mathematically
 463 restricted at the upper bound, d_u . n_u is usually smaller than mean value in the size range from d_k to d_u during a NPF event, and
 464 recent work have revealed that the observed GR is size dependent (Kuang et al., 2012; Kulmala et al., 2013; Xiao et al., 2015).
 465 For example, as shown in Fig. B2, GR varies with time in the NPF event on Apr. 3rd, 2016, and was linearly fitted in different
 466 diameter ranges. The mean GR of particles ranged from 2 nm to 25 nm is ~7.47 nm/h, while GR_{25} is ~10.86 nm/h. At 11:30
 467 on Apr. 3rd, n_{25} ($dN/d\log d_p$ at 25 nm) is 164 #/cm³, while the mean n of particles ranged from 2 nm to 25 nm is 4755 #/cm³.
 468 The calculated condensational growth term in Eq. (B6) is ~20 times of that in Eq. (A13).

469 In relatively clean environment with weak NPF events, Eq. (B6) may work well since the calculated J_k is mainly predominated
 470 by dN/dt . However, when number concentration of aerosol formed by nucleation and (or) background aerosol is high, i.e.,
 471 when $CoagS_{nk}$ is the major component of J_k , Eq. (B6) underestimates the formation rate (and nucleation rate) due to
 472 underestimation of the coagulation scavenging effect.

473

474 **Acknowledgement**

475 Financial supports from the National Science Foundation of China (21422703, 41227805 & 21521064) and the National Key
 476 R&D Program of China (2014BAC22B00 & 2016YFC0200102) are appreciated.

- 478 Aitken, J.: On some nuclei of cloudy nucleation, *Proceedings of the Royal Society of Edinburgh*, XXXI, 495-511, 1911.
- 479 An, J., Wang, H., Shen, L., Zhu, B., Zou, J., Gao, J., and Kang, H.: Characteristics of new particle formation events in Nanjing, China: Effect
480 of water-soluble ions, *Atmospheric Environment*, 108, 32-40, doi:10.1016/j.atmosenv.2015.01.038, 2015.
- 481 Cai, R., Chen, D.-R., Hao, J., and Jiang, J.: A miniature cylindrical differential mobility analyzer for sub-3 nm particle sizing, *Journal of*
482 *Aerosol Science*, 106, 111-119, doi:10.1016/j.jaerosci.2017.01.004, 2017.
- 483 Cao, C., Jiang, W., Wang, B., Fang, J., Lang, J., Tian, G., Jiang, J., and Zhu, T. F.: Inhalable microorganisms in Beijing's PM_{2.5} and PM₁₀
484 pollutants during a severe smog event, *Environmental science & technology*, 48, 1499-1507, doi:10.1021/es4048472, 2014.
- 485 Clarke, A. D., Davis, D., Kapustin, V. N., Eisele, F., Chen, G., Paluch, I., Lenschow, D., Bandy, A. R., Thornton, D., Moore, K., Mauldin,
486 L., Tanner, D., Litchy, M., Carroll, M. A., Collins, J., and Albercook, G.: Particle nucleation in the tropical boundary layer and its
487 coupling to marine sulfur sources, *Science*, 282, 89-92, doi:10.1126/science.282.5386.89, 1998.
- 488 Covert, D. S., Kapustin, V. N., Quinn, P. K., and Bates, T. S.: New particle formation in the marine boundary layer, *Journal of Geophysical*
489 *Research*, 97, 20518-20589, 1992.
- 490 Covert, D. S., Wiedensohler, A., Aalto, P., Heintzenberg, J., McMurry, P. H., and Leck, C.: Aerosol number size distributions from 3 to 500
491 nm diameter in the arctic marine boundary layer during summer and autumn, *Tellus B*, 48, doi:10.1034/j.1600-0889.1996.t01-1-
492 00005.x, 1996.
- 493 Dal Maso, M., Kulmala, M., Riipinen, I., Wagner, R., Hussein, T., Aalto, P., and Lehtinen, K. E.: Formation and growth of fresh atmospheric
494 aerosols: eight years of aerosol size distribution data from SMEAR II, Hyytiälä, Finland, *Boreal Environment Research*, 10, 323-
495 336, 2005.
- 496 Franchin, A., Downard, A., Kangasluoma, J., Nieminen, T., Lehtipalo, K., Steiner, G., Manninen, E. H., Petäjä, T., Flagan, R. C., and
497 Kulmala, M.: A new high-transmission inlet for the Caltech nano-RDMA for size distribution measurements of sub-3 nm ions at
498 ambient concentrations, *Atmospheric Measurement Techniques*, 9, 2709-2720, doi:10.5194/amt-9-2709-2016, 2016.
- 499 Friedlander, S. K.: Smoke, dust and haze, 2nd ed., *Topics in Chemical Engineering*, edited by: Gubbins, K. E., Oxford University Press,
500 New York, 2000.
- 501 Hagen, D. E., and Alofs, D. J.: Linear Inversion Method to Obtain aerosol Size Distributions from Measurements with a Differential Mobility
502 Analyzer, *Aerosol Science and Technology*, 2, 465-475, 1983.
- 503 He, K., Yang, F., Ma, Y., Zhang, Q., Yao, X., Chan, C. K., Cadel, S., Chan, T., and Mulawa, P.: The characteristics of PM_{2.5} in Beijing,
504 China, *Atmospheric Environment*, 35, 4959-4970, 2001.
- 505 Heisler, S. L., and Friedlander, S. K.: Gas-to-particle conversion in photochemical smog: Aerosol growth laws and mechanisms for organics,
506 *Atmospheric Environment*, 11, 157-168, doi:10.1016/0004-6981(77)90220-7, 1977.
- 507 Hu, M., Peng, J., Sun, K., Yue, D., Guo, S., Wiedensohler, A., and Wu, Z.: Estimation of size-resolved ambient particle density based on
508 the measurement of aerosol number, mass, and chemical size distributions in the winter in Beijing, *Environmental science &*
509 *technology*, 46, 9941-9947, doi:10.1021/es204073t, 2012.
- 510 Iida, K., Stolzenburg, M., McMurry, P., Dunn, M. J., Smith, J. N., Eisele, F., and Keady, P.: Contribution of ion-induced nucleation to new
511 particle formation: Methodology and its application to atmospheric observations in Boulder, Colorado, *Journal of Geophysical*
512 *Research: Atmospheres*, 111, D23201, doi:10.1029/2006jd007167, 2006.
- 513 Iida, K., Stolzenburg, M. R., McMurry, P. H., and Smith, J. N.: Estimating nanoparticle growth rates from size-dependent charged fractions:
514 Analysis of new particle formation events in Mexico City, *Journal of Geophysical Research: Atmospheres*, 113,
515 doi:10.1029/2007jd009260, 2008.
- 516 Iida, K., Stolzenburg, M. R., and McMurry, P. H.: Effect of Working Fluid on Sub-2 nm Particle Detection with a Laminar Flow Ultrafine
517 Condensation Particle Counter, *Aerosol Science and Technology*, 43, 81-96, doi:10.1080/02786820802488194, 2009.
- 518 Jiang, J., Chen, M., Kuang, C., Attoui, M., and McMurry, P. H.: Electrical Mobility Spectrometer Using a Diethylene Glycol Condensation
519 Particle Counter for Measurement of Aerosol Size Distributions Down to 1 nm, *Aerosol Science and Technology*, 45, 510-521,
520 doi:10.1080/02786826.2010.547538, 2011a.

521 Jiang, J., Zhao, J., Chen, M., Eisele, F. L., Scheckman, J., Williams, B. J., Kuang, C., and McMurry, P. H.: First Measurements of Neutral
522 Atmospheric Cluster and 1–2 nm Particle Number Size Distributions During Nucleation Events, *Aerosol Science and Technology*,
523 45, ii-v, doi:10.1080/02786826.2010.546817, 2011b.

524 Kerminen, V.-M., Paramonov, M., Anttila, T., Riipinen, I., Fountoukis, C., Korhonen, H., Asmi, E., Laakso, L., Lihavainen, H., Swietlicki,
525 E., Svenningsson, B., Asmi, A., Pandis, S. N., Kulmala, M., and Petäjä, T.: Cloud condensation nuclei production associated with
526 atmospheric nucleation: a synthesis based on existing literature and new results, *Atmospheric Chemistry and Physics*, 12, 12037-
527 12059, doi:10.5194/acp-12-12037-2012, 2012.

528 Kuang, C., Chen, M., Zhao, J., Smith, J., McMurry, P. H., and Wang, J.: Size and time-resolved growth rate measurements of 1 to 5 nm
529 freshly formed atmospheric nuclei, *Atmospheric Chemistry and Physics*, 12, 3573-3589, doi:10.5194/acp-12-3573-2012, 2012.

530 Kuang, C., McMurry, P. H., and McCormick, A. V.: Determination of cloud condensation nuclei production from measured new particle
531 formation events, *Geophysical Research Letters*, 36, doi:10.1029/2009gl037584, 2009.

532 Kuang, C., McMurry, P. H., McCormick, A. V., and Eisele, F. L.: Dependence of nucleation rates on sulfuric acid vapor concentration in
533 diverse atmospheric locations, *Journal of Geophysical Research*, 113, doi:10.1029/2007jd009253, 2008.

534 Kuang, C., Riipinen, I., Sihto, S. L., Kulmala, M., McCormick, A. V., and McMurry, P. H.: An improved criterion for new particle formation
535 in diverse atmospheric environments, *Atmospheric Chemistry and Physics*, 10, 8469-8480, doi:10.5194/acp-10-8469-2010, 2010.

536 Kulmala, M., Dal Maso, M., Mäkelä, J. M., Pirjola, L., Väkevä, M., Aalto, P., Miikkulainen, P., Hämeri, K., and O'dowd, C. D.: On the
537 formation, growth and composition of nucleation mode particles, *Tellus*, 53, 479-490, 2001.

538 Kulmala, M., Kontkanen, J., Junninen, H., Lehtipalo, K., Manninen, H. E., Nieminen, T., Petäjä, T., Sipilä, M., Schobesberger, S., Rantala,
539 P., Franchin, A., Jokinen, T., Jarvinen, E., Äijälä, M., Kangasluoma, J., Hakala, J., Aalto, P. P., Paasonen, P., Mikkilä, J.,
540 Vanhanen, J., Aalto, J., Hakola, H., Makkonen, U., Ruuskanen, T., Mauldin, R. L., 3rd, Duplissy, J., Vehkamäki, H., Bäck, J.,
541 Kortelainen, A., Riipinen, I., Kurtén, T., Johnston, M. V., Smith, J. N., Ehn, M., Mentel, T. F., Lehtinen, K. E., Laaksonen, A.,
542 Kerminen, V.-M., and Worsnop, D. R.: Direct observations of atmospheric aerosol nucleation, *Science*, 339, 943-946,
543 doi:10.1126/science.1227385, 2013.

544 Kulmala, M., Petäjä, T., Kerminen, V. M., Kujansuu, J., Ruuskanen, T., Ding, A. J., Nie, W., Hu, M., Wang, Z., Wu, Z., Wang, L., and
545 Worsnop, D. R.: On secondary new particle formation in China, *Frontiers of Environmental Science & Engineering*, 10, 191-200,
546 doi:10.1007/s11783-016-0850-1, 2016.

547 Kulmala, M., Petäjä, T., Mönkkönen, P., Koponen, I. K., Dal Maso, M., Aalto, P. P., Lehtinen, K. E., and Kerminen, V. M.: On the growth
548 of nucleation mode particles: source rates of condensable vapor in polluted and clean environments, *Atmospheric Chemistry and
549 Physics*, 5, 409-416, 2005.

550 Kulmala, M., Petäjä, T., Nieminen, T., Sipilä, M., Manninen, H. E., Lehtipalo, K., Dal Maso, M., Aalto, P. P., Junninen, H., Paasonen, P.,
551 Riipinen, I., Lehtinen, K. E., Laaksonen, A., and Kerminen, V. M.: Measurement of the nucleation of atmospheric aerosol particles,
552 *Nature protocols*, 7, 1651-1667, doi:10.1038/nprot.2012.091, 2012.

553 Kulmala, M., Vehkamäki, H., Petäjä, T., Dal Maso, M., Lauri, A., Kerminen, V. M., Birmili, W., and McMurry, P. H.: Formation and growth
554 rates of ultrafine atmospheric particles: a review of observations, *Journal of Aerosol Science*, 35, 143-176,
555 doi:10.1016/j.jaerosci.2003.10.003, 2004.

556 Lee, S.-H., Reeves, J. M., Wilson, J. C., Hunton, D. E., Viggiano, A. A., Miller, T. M., Ballenthin, J. O., and Lait, L. R.: Particle formation
557 by ion nucleation in the upper troposphere and lower stratosphere, *Science*, 301, 1886-1889, doi:10.1126/science.1087236, 2003.

558 Lehtinen, K. E. J., Dal Maso, M., Kulmala, M., and Kerminen, V.-M.: Estimating nucleation rates from apparent particle formation rates
559 and vice versa: Revised formulation of the Kerminen–Kulmala equation, *Journal of Aerosol Science*, 38, 988-994,
560 doi:10.1016/j.jaerosci.2007.06.009, 2007.

561 Lehtipalo, K., Leppä, J., Kontkanen, J., Kangasluoma, J., Franchin, A., Wimmer, D., Schobesberger, S., Junninen, H., Petäjä, T., Sipilä, M.,
562 Mikkilä, J., Vanhanen, J., Worsnop, D. R., and Kulmala, M.: Methods for determining particle size distribution and growth rates
563 between 1 and 3 nm using the Particle Size Magnifier, *Boreal Environment Research*, 19, 215-236, 2014.

564 Leng, C., Zhang, Q., Tao, J., Zhang, H., Zhang, D., Xu, C., Li, X., Kong, L., Cheng, T., Zhang, R., Yang, X., Chen, J., Qiao, L., Lou, S.,
565 Wang, H., and Chen, C.: Impacts of new particle formation on aerosol cloud condensation nuclei (CCN) activity in Shanghai: case
566 study, *Atmospheric Chemistry and Physics*, 14, 11353-11365, doi:10.5194/acp-14-11353-2014, 2014.

567 Liu, J., Jiang, J., Zhang, Q., Deng, J., and Hao, J.: A spectrometer for measuring particle size distributions in the range of 3 nm to 10 μm ,
568 *Frontiers of Environmental Science & Engineering*, 10, 63-72, doi:10.1007/s11783-014-0754-x, 2016.

569 Lohmann, U., and Feichter, J.: Global indirect aerosol effects: a review, *Atmospheric Chemistry and Physics*, 5, 715–737, doi:10.5194/acp-
570 5-715-2005, 2005.

571 Manninen, E. H., Nieminen, T., Riipinen, I., Yli-Juuti, T., Gagné, S., Asmi, E., Aalto, P. P., Petäjä, T., Kerminen, V.-M., and Kulmala, M.:
572 Charged and total particle formation and growth rates during EUCAARI 2007 campaign in Hyytiälä, *Atmospheric Chemistry and*
573 *Physics*, 9, 4077-4089, doi:10.5194/acp-9-4077-2009, 2009.

574 McMurry, P. H.: New particle formation in the presence of an aerosol: rates, time scales, and sub-0.01 μm size distributions *Journal of*
575 *Colloid and Interface Science*, 95, 72-80, 1983.

576 McMurry, P. H., Fink, M., Sakurai, H., Stolzenburg, M. R., Mauldin, R. L., Smith, J., Eisele, F., Moore, K., Sjostedt, S., Tanner, D., Huey,
577 L. G., Nowak, J. B., Edgerton, E., and Voisin, D.: A criterion for new particle formation in the sulfur-rich Atlanta atmosphere,
578 *Journal of Geophysical Research*, 110, doi:10.1029/2005jd005901, 2005.

579 Misaki, M.: Mobility spectrums of large ions in the new Mexico semidesert, *Journal of Geophysical Research*, 69, 3309-3318, 1964.

580 Paasonen, P., Sihto, S.-L., Nieminen, T., Vuollekoski, H., Riipinen, I., Plaß-Dülmer, C., Berresheim, H., Birmili, W., and Kulmala, M.:
581 Connection between new particle formation and sulphuric acid at Hohenpeissenberg (Germany) including the influence of organic
582 compounds, *Boreal Environment Research*, 14, 616-629, 2009.

583 Park, J., Sakurai, H., Vollmers, K., and McMurry, P. H.: Aerosol size distributions measured at the South Pole during ISCAT, *Atmospheric*
584 *Environment*, 38, 5493-5500, doi:10.1016/j.atmosenv.2002.12.001, 2004.

585 Qi, X. M., Ding, A. J., Nie, W., Petäjä, T., Kerminen, V.-M., Herrmann, E., Xie, Y. N., Zheng, L. F., Manninen, H., Aalto, P., Sun, J. N.,
586 Xu, Z. N., Chi, X. G., Huang, X., Boy, M., Virkkula, A., Yang, X.-Q., Fu, C. B., and Kulmala, M.: Aerosol size distribution and
587 new particle formation in the western Yangtze River Delta of China: 2 years of measurements at the SORPES station, *Atmospheric*
588 *Chemistry and Physics*, 15, 12445-12464, doi:10.5194/acp-15-12445-2015, 2015.

589 Riipinen, I., Sihto, S.-L., Kulmala, M., Arnold, F., Dal Maso, M., Birmili, W., Saarnio, K., Teinilä, K., Kerminen, V.-M., Laaksonen, A.,
590 and Lehtinen, K. E. J.: Connections between atmospheric sulphuric acid and new particle formation during QUEST III-IV
591 campaigns in Heidelberg and Hyytiälä, *Atmospheric Chemistry and Physics*, 7, 1899-1914, doi:10.5194/acpd-6-10837-2006,
592 2007.

593 Seinfeld, J. H., and Pandis, S. N.: *Atmospheric Chemistry and Physics*, 2nd ed., John Wiley & Sons, Inc., New Jersey, 2006.

594 Shen, X. J., Sun, J. Y., Zhang, Y. M., Wehner, B., Nowak, A., Tuch, T., Zhang, X. C., Wang, T. T., Zhou, H. G., Zhang, X. L., Dong, F.,
595 Birmili, W., and Wiedensohler, A.: First long-term study of particle number size distributions and new particle formation events
596 of regional aerosol in the North China Plain, *Atmospheric Chemistry and Physics*, 11, 1565-1580, doi:10.5194/acp-11-1565-2011,
597 2011.

598 Sihto, S.-L., Kulmala, M., Kerminen, V.-M., Dal Maso, M., Petäjä, T., Riipinen, I., Korhonen, H., Arnold, F., Janson, R., Boy, M.,
599 Laaksonen, A., and Lehtinen, K. E.: Atmospheric sulphuric acid and aerosol formation: implications from atmospheric
600 measurements for nucleation and early growth mechanisms, *Atmospheric Chemistry and Physics*, 6, 4079-4091, doi:10.5194/acp-
601 6-4079-2006, 2006.

602 Vanhanen, J., Mikkilä, J., Lehtipalo, K., Sipilä, M., Manninen, H. E., Siivola, E., Petäjä, T., and Kulmala, M.: Particle Size Magnifier for
603 Nano-CN Detection, *Aerosol Science and Technology*, 45, 533-542, doi:10.1080/02786826.2010.547889, 2011.

604 Vuollekoski, H., Sihto, S.-L., Kerminen, V.-M., Kulmala, M., and Lehtinen, K. E. J.: A numerical comparison of different methods for
605 determining the particle formation rate, *Atmospheric Chemistry and Physics*, 12, 2289-2295, doi:10.5194/acp-12-2289-2012,
606 2012.

607 Wang, Z. B., Hu, M., Pei, X. Y., Zhang, R. Y., Paasonen, P., Zheng, J., Yue, D. L., Wu, Z. J., Boy, M., and Wiedensohler, A.: Connection
608 of organics to atmospheric new particle formation and growth at an urban site of Beijing, *Atmospheric Environment*, 103, 7-17,
609 doi:10.1016/j.atmosenv.2014.11.069, 2015.

610 Wang, Z. B., Hu, M., Sun, J. Y., Wu, Z. J., Yue, D. L., Shen, X. J., Zhang, Y. M., Pei, X. Y., Cheng, Y. F., and Wiedensohler, A.:
611 Characteristics of regional new particle formation in urban and regional background environments in the North China Plain,
612 *Atmospheric Chemistry and Physics*, 13, 12495-12506, doi:10.5194/acp-13-12495-2013, 2013.

613 Wang, Z. B., Hu, M., Yue, D. L., Zheng, J., Zhang, R. Y., Wiedensohler, A., Wu, Z. J., Nieminen, T., and Boy, M.: Evaluation on the role
614 of sulfuric acid in the mechanisms of new particle formation for Beijing case, *Atmospheric Chemistry and Physics*, 11, 12663-
615 12671, doi:10.5194/acp-11-12663-2011, 2011.

616 Wang, Z., Wu, Z., Yue, D., Shang, D., Guo, S., Sun, J., Ding, A., Wang, L., Jiang, J., Guo, H., Gao, J., Cheung, H. C., Morawska, L.,
617 Keywood, M., and Hu, M.: New particle formation in China: Current knowledge and further directions, *The Science of the total*
618 *environment*, 577, 258-266, doi:10.1016/j.scitotenv.2016.10.177, 2017.

619 Weber, R. J., Marti, J. J., McMurry, P. H., Eisele, F. L., Tanner, D. J., and Jefferson, A.: Measured atmospheric new particle formation rates:
620 implications for nucleation mechanisms, *Chemical Engineering Communications*, 151, 53-64, doi:10.1080/00986449608936541,
621 1996.

622 Weber, R. J., Marti, J. J., McMurry, P. H., Eisele, F. L., Tanner, D. J., and Jefferson, A.: Measurements of new particle formation and
623 ultrafine particle growth rates at a clean continental site, *Journal of Geophysical Research: Atmospheres*, 102, 4375-4385,
624 doi:10.1029/96jd03656, 1997.

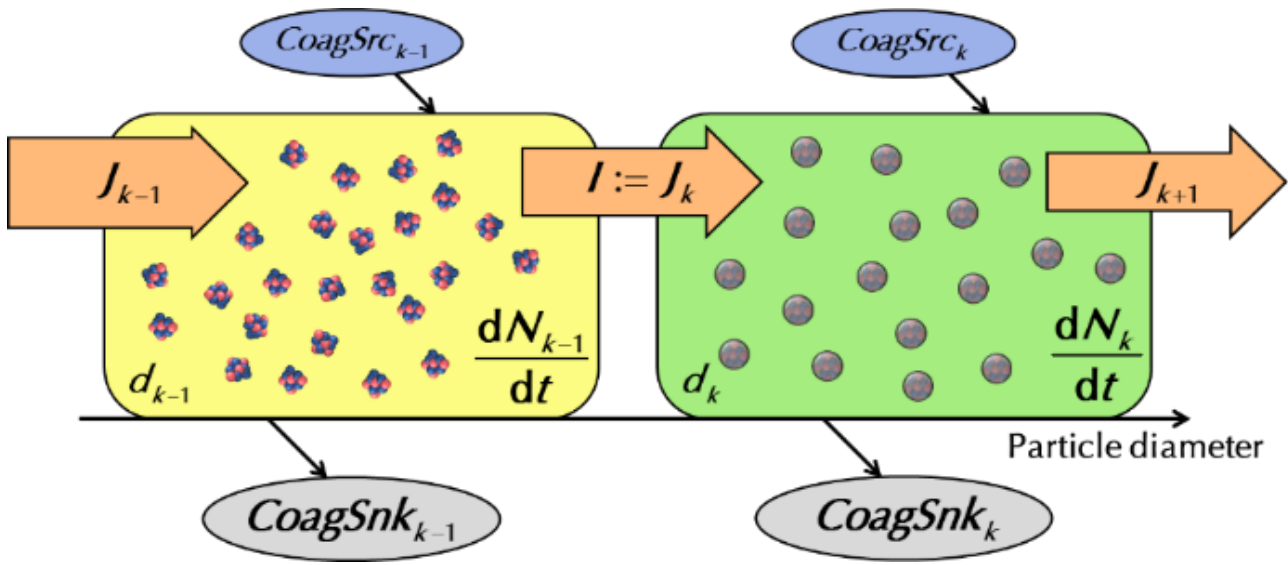
625 Wu, Z., Hu, M., Liu, S., Wehner, B., Bauer, S., Maßling, A., Wiedensohler, A., Petäjä, T., Dal Maso, M., and Kulmala, M.: New particle
626 formation in Beijing, China: Statistical analysis of a 1-year data set, *Journal of Geophysical Research*, 112,
627 doi:10.1029/2006jd007406, 2007.

628 Xiao, S., Wang, M. Y., Yao, L., Kulmala, M., Zhou, B., Yang, X., Chen, J. M., Wang, D. F., Fu, Q. Y., Worsnop, D. R., and Wang, L.:
629 Strong atmospheric new particle formation in winter in urban Shanghai, China, *Atmospheric Chemistry and Physics*, 15, 1769-
630 1781, doi:10.5194/acp-15-1769-2015, 2015.

631 Yue, D., Hu, M., Wu, Z., Wang, Z., Guo, S., Wehner, B., Nowak, A., Achtert, P., Wiedensohler, A., Jung, J., Kim, Y. J., and Liu, S.:
632 Characteristics of aerosol size distributions and new particle formation in the summer in Beijing, *Journal of Geophysical Research*,
633 114, doi:10.1029/2008jd010894, 2009.

634 Zhou, J.: Submicrometer aerosol particle size distribution and hygroscopic growth measured in the Amazon rain forest during the wet season,
635 *Journal of Geophysical Research*, 107, doi:10.1029/2000jd000203, 2002.

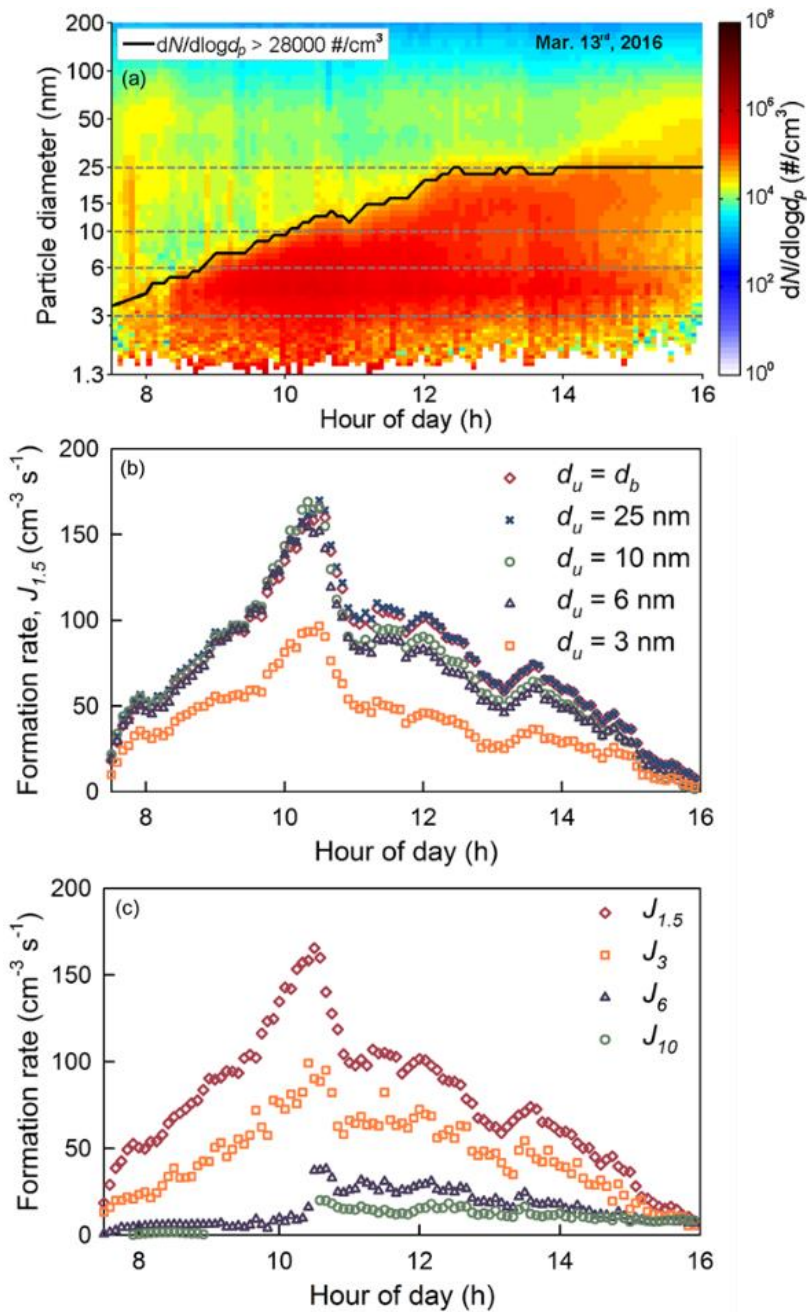
636



637

638 **Figure 1: Schematic of the general dynamic equation.**

639



640

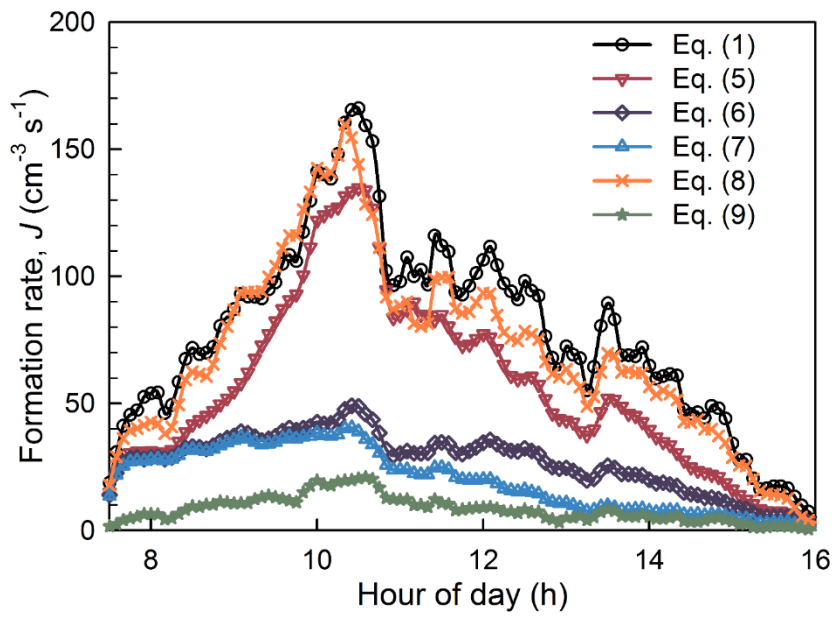
641 **Figure 2: Comparison of formation rates estimated using different upper bounds, d_u . (a) A typical new particle formation event.**

642 **Dashed gray lines represent different d_u in Eq. (1). Solid black lines corresponds to d_b , i.e., the varying upper bound determined by**

643 **$dN/d\log d_p$. (b) Estimated formation rates with different upper bound, d_u , using Eq. (1). (c) Estimated formation rates with different**

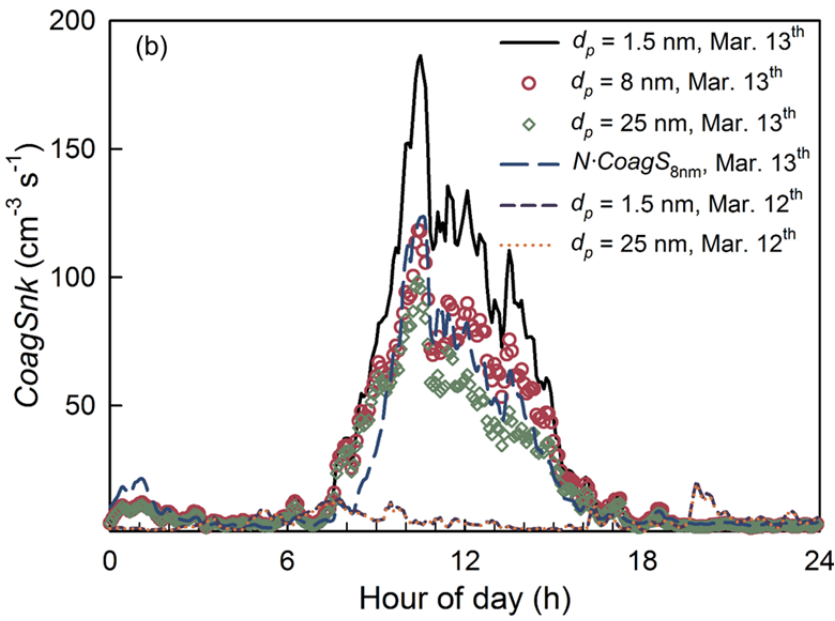
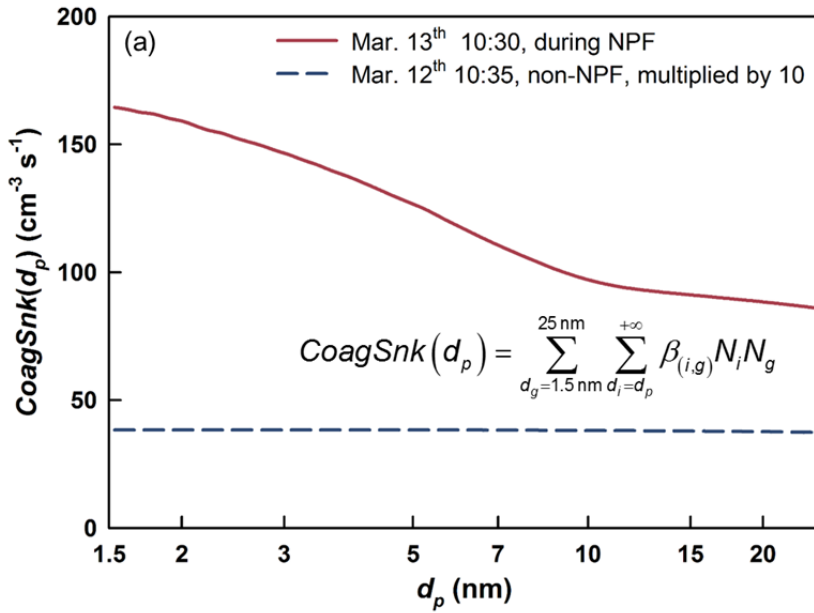
644 **d_k using Eq. (1). d_u equals 25 nm and d_{min} equals 1.3 nm in the four scatter plots.**

645



646
 647 **Figure 3: Comparison of formation rates estimated by different formulae.**

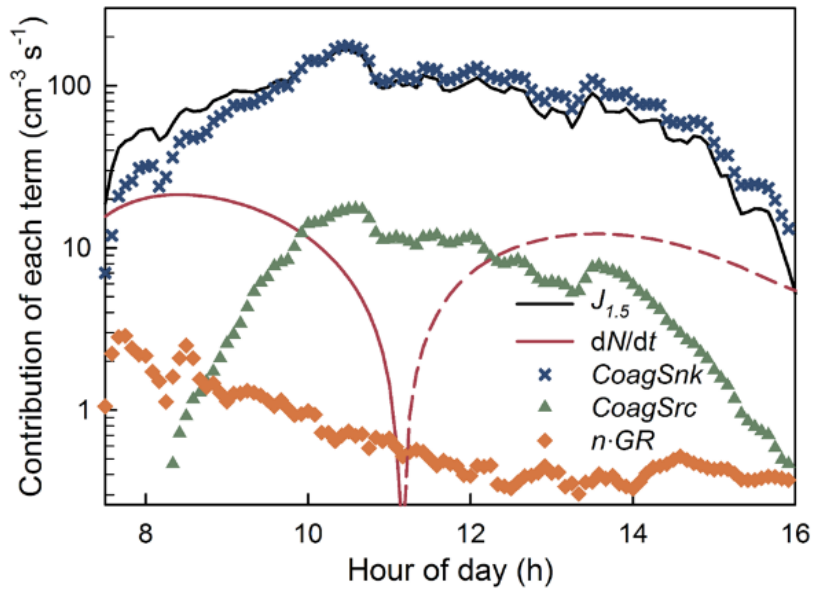
648



649

650 **Figure 4:** (a) $CoagSnk$ as a function of d_p , where d_p is the accounted minimum diameter when calculating $CoagS_g$ for particles at all
 651 different d_g , and scavenging due to coagulation with particles smaller than d_p is neglected, as the defined by the formula in panel (a).
 652 The dashed line corresponding to $CoagSnk$ on a non-NPF day is also monotonously decreasing with the increase of d_{min} by a negligible
 653 slope. (b) Time evolution of $CoagSnk$ versus time on a NPF day (Mar. 13th) and a non-NPF day (Mar. 12th). d_p is defined the same
 654 same with that in panel (a). N is the number concentration of particles in the size range from 1.5 nm to 25 nm, while $CoagS_{8nm}$ is calculated
 655 using Eq. (3).

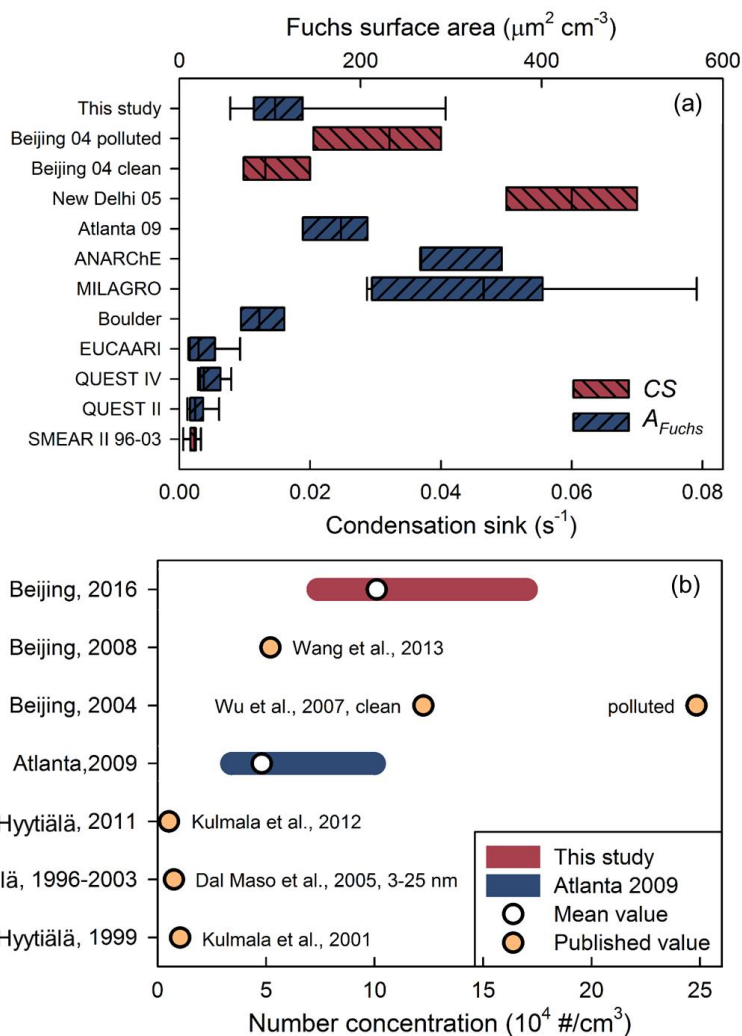
656



657

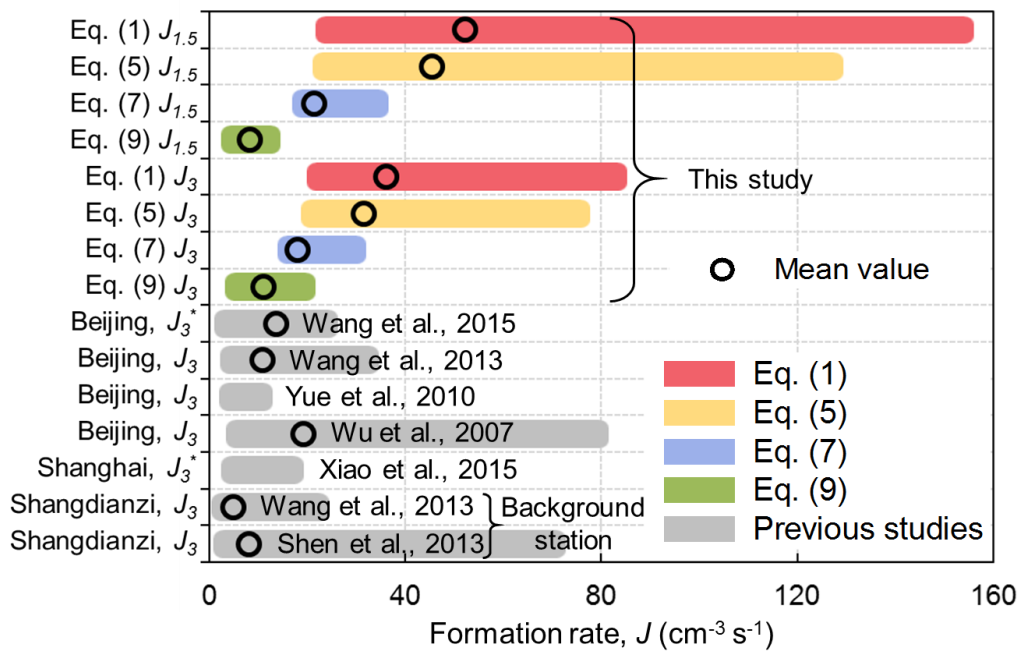
658 **Figure 5: Contribution of each term to the estimated formation rate. dN/dt is obtained by fitting and shown in absolute value with**
 659 **solid and dashed lines corresponding to positive and negative parts, respectively. Note the upper bound, d_u , equals d_b as defined**
 660 **section 4.1 for better accuracy, however, it doesn't affect the generality of the result.**

661



662
663
664
665
666
667
668
669
670
671

Figure 6: (a) Comparison of Fuchs surface area and condensation sink in Beijing (when NPF events occurred) with those in other locations. NPF days were classified by condensation sink in urban Beijing in 2004 (Wu et al., 2007). Condensation sink on NPF days in New Delhi was reported by Kulmala et al. (2005). ANARChE (McMurry et al., 2005) and MILAGRO (Iida et al., 2008) were conducted in Atlanta and Tecamac, respectively, while EUCCARI (Manninen et al., 2009), QUEST II (Sihto et al., 2006), QUEST IV (Riipinen et al., 2007) was conducted in SMEAR II (Dal Maso et al., 2005), Hyytiälä. A_{Fuchs} data in MILAGRO, ANARChE, Boulder, EUCCARI, QUEST II, and QUEST IV were published in Kuang et al. (2010). The ends of coloured rectangular correspond quartiles, while error bar represents the 10th and 90th percent value. (b) Comparison of peak number concentration of particles larger than 3 nm during NPF events in this study with those in Atlanta and other published data. Note that the published values (light orange points) in previous studies are not necessarily the mean values of the whole campaign periods.



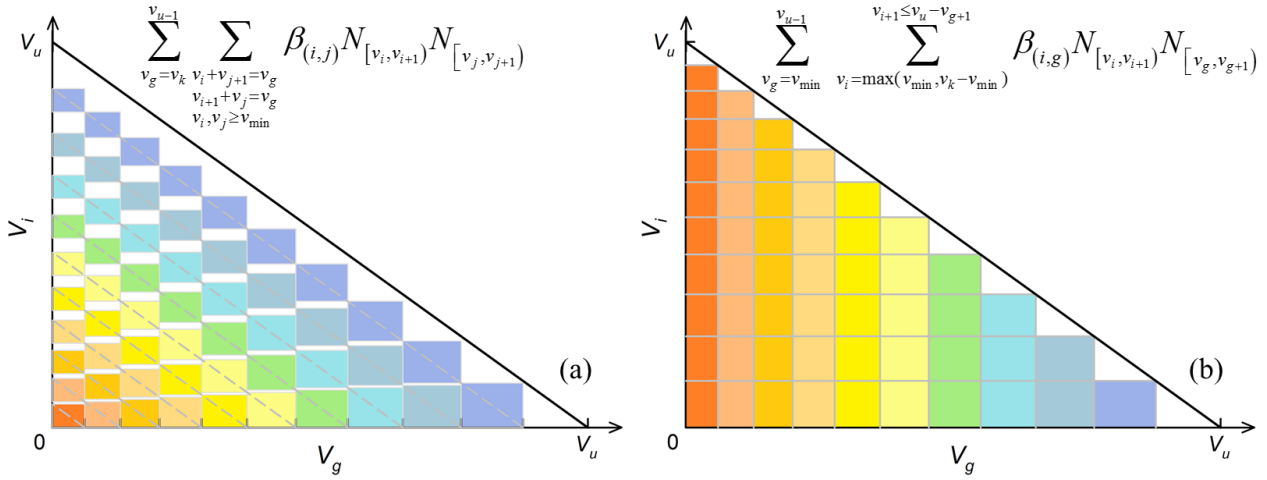
672

673

674

675

Figure 7: Estimated $J_{1.5}$ and J_3 using different equations. Previously reported J_3 in China were included for comparison. The ends of coloured rectangular correspond to the minimum value and the maximum value, respectively. *: The upper size bound to estimate formation rate, d_u , is 6 nm (rather than 25 nm) in Wang et al., 2015 and Xiao et al., 2015.



676

677

678

679

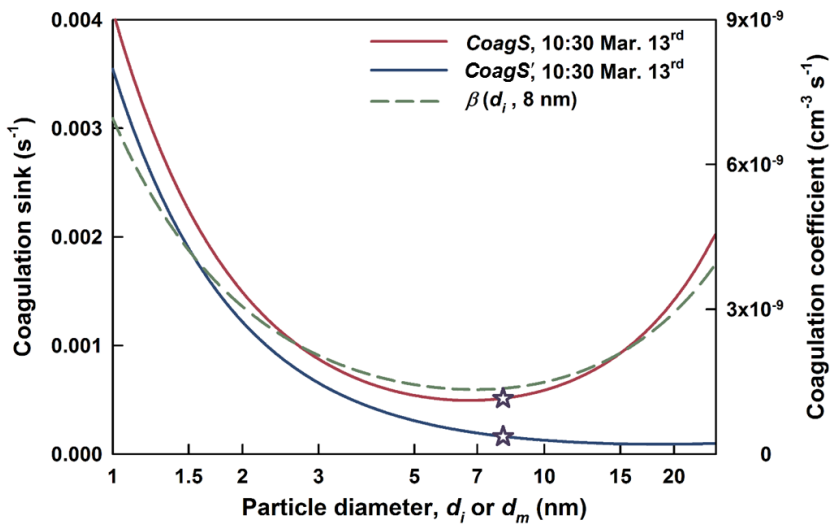
680

681

682

683

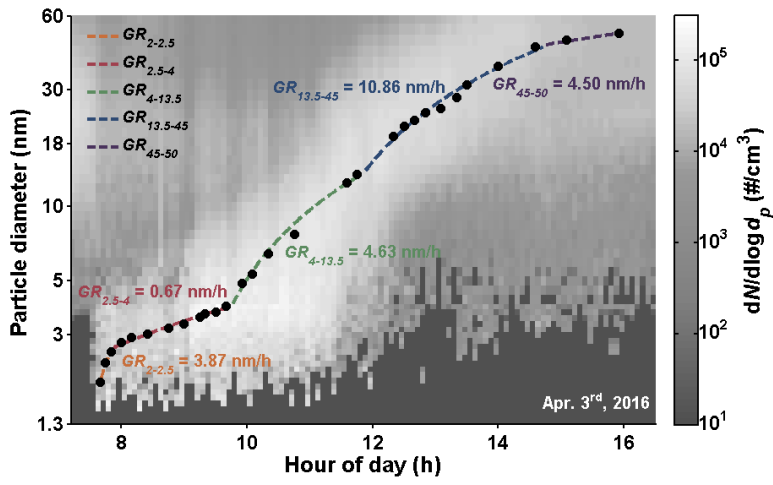
Figure A1: Figure A1: Schematic for two different summation sequences to estimate the coagulation source term. Equations in panels (a) and (b) correspond to the continuous forms of the far LHS and the far RHS formulae in Eq. (A7), respectively. The coagulation source term is denoted by half the area of the triangle (since the particles at the same diameter are accounted for twice). The colored areas are the estimated area using the two equations, respectively. The summation terms corresponding to the same particle volume, v_g , are shown in the same color. The coagulation source term is underestimated in panel (a) because v_g increases nonlinearly in this case, whereas the estimated coagulation source term is independent of the bin structures for d_g and d_i in panel (b).



684

685 **Figure B1:** Coagulation coefficient and calculated coagulation sink during a typical NPF event. *CoagS* and *CoagS'* are defined in
 686 Eq. (B7) and Eq. (B8), respectively, and d_m in this figure is treated as a variable rather than a constant value. The upper and lower
 687 star denote $CoagS'_{\delta_{nm}}$ and $CoagS_{\delta_{nm}}$ which are used in the second term in the RHS of Eq. (5) and Eq. (6) to approximate *CoagS_{nk}*,
 688 respectively.

689



690

691 **Figure B2: Size and time dependent growth rate on a NPF day observed in Beijing. Representative diameters are obtained by**
 692 **lognormal fitting of nucleation mode particles in each time bin, and GR is linearly fitted in each section.**

693